Catalytic hydrodenitrogenation of primary, secondary, and tertiary C12-alkyl amines over a platinum on zirconia catalyst

Leoni-Franziska Klingelhöfer[a,b], Joakim Kattelus*[a], Emma Verkama[a,c], Jorge Velasco[a], Leonhard Iser[b], Marcus Rose[b], Reetta Karinen[a], Riikka L. Puurunen[a]

In this work, the hydrodenitrogenation (HDN) of a primary amine (dodecylamine), a secondary amine (didodecylamine), and a tertiary amine (tridodecylamine) over a Pt/ZrO_2 catalyst was compared in a batch reactor. The main product of the amine hydrotreating was dodecane, but significant amounts of secondary amine were also formed as an intermediate during HDN of the primary and the tertiary amine. It was found that the primary amine is the only species for which direct HDN is possible; HDN of the secondary amine thus proceeds through a primary amine intermediate and HDN of the tertiary amine involves formation of secondary amine, which decomposes to primary amine. Consequently, HDN of the tertiary and secondary amines is slower than that of the primary amine. Kinetic modeling indicated that bimolecular condensation reactions of the primary amine, as well as potentially of the primary amine and the secondary amine, have a significant effect on the HDN process. Formation of secondary amine from primary amine increases the initial conversion and nitrogen removal rate but appeared to slow down the overall rate of nitrogen removal. The results thus demonstrate how condensation reactions affect amine HDN, which has implications for catalyst design for HDN of renewable feeds containing aliphatic amines.

[a.] *Aalto University, School of Chemical Engineering.*
[b.] *Technische Universität Darmstadt, Department of Chemistry.*
[c.] *Present address for E.Verkama: Fraunhofer Institute for Solar Energy Systems ISE, Heidenhofstr. 2, 79110 Freiburg, Germany*

Introduction

Replacing fossil fuels with sustainable, renewable options is an important strategy for lowering CO_2 emissions and reducing the impact of the transportation sector on global warming. While electrification shows great promise in reducing emissions for the transportation sector in general, finding sustainable options for the aviation sector is particularly challenging, due to the need for fuels with a high-energy density.[1] Sustainable, bio-based fuels are thus a particularly promising option for the aviation sector.[1] According to the International Air Transportation Association[2], bio-based fuels are estimated to contribute up to 65 % to the reduction of greenhouse gas emission in the aviation sector by 2050. High energy density drop-in fuels can be used in existing fleet, and thus make the transition towards a sustainable economy easier. The European Commission passed a mandate on 18 October 2023 for blending fossil based fuel with sustainable aviation fuel (SAF) gradually from 2 % in 2025 to 63 % in 2050[3]. Estimates made by Klöwer et al.[4] emphasize the importance of increasing the production of renewable fuels even faster, as an increase of bio-based fuels up to 90 % by 2050 is needed to limit aviation transport effects on global warming.

Hydrotreating is a commercially viable process to produce bio-based fuels from renewable feedstocks.[5,6] For example, Neste Corporation and Eni S.p.A. commercially produce diesel and jet fuel from vegetable oils and fats via hydrotreating.[6–8] Likewise, hydrotreating is a viable strategy to upgrade bio-based feedstocks produced through pyrolysis or liquefaction of biomass.[5,9] During hydrotreating, heteroatoms, such as S, N, and O, are removed in the form of, H_2S, NH_3, H_2O, CO_2 and CO by contacting the feedstock with hydrogen in the presence of a catalyst.[5,6] Oxygen-containing compounds, which are prevalent in renewable feedstocks, lower the pH value, cause corrosion, polymerization and fuel instability.[10] Nitrogen-containing compounds can poison acidic catalysts in downstream processes such as reforming, hydrocracking and hydroisomerization, as well as impact the fuel stability negatively.[5,11,12]

With the change from fossil to bio-based feedstock, the composition of the hydrotreating feed differs, especially regarding the oxygen and nitrogen content but also the types of compounds present. For example, algae-based feeds can contain up to 35 wt% oxygen and up to 10 wt% nitrogen, while for bio-oils from pyrolysis and liquefaction, the heteroatom content can range between 9-38 wt% oxygen and 6-10 wt% nitrogen.[5,6,9,13] In comparison, fossil-based feeds usually contain less than 2 wt% oxygen and less than 1 wt-% nitrogen.[9,14] This change in feed composition has led to an increasing interest in hydrodeoxygenation (HDO).[9,15–17] However, as removing the nitrogen has been shown to be more difficult, studying hydrodenitrogenation (HDN) is of equal importance.[18] In bio-based feedstocks like vegetable oils, animal fats, and algae, nitrogen is mostly found in form of fatty amides, alkyl amines, cyclic amines, and amino acids.[5,12,19–21]

Supported noble metal catalysts, such as Ru, Rh, Pd, Pt, have been shown to be active in HDO and HDN of fatty acids, amides and amines.[18,22–30] They show high HDO/HDN activity under mild conditions, with the metal identity significantly impacting

the product selectivity.[11,22,29–31] As noble metal catalysts are active in their reduced state, they, in contrast to the commercially used transition metal sulfide catalysts, do not require sulfur additions to maintain their activity.[5,9,11,18,22,24,31,32] For HDN of amines and amides, reduced noble metal catalysts display activity towards the formation of ammonia and paraffins.[22,23,26] Secondary dialkylamines are also readily formed over most of the studied metals.[18,22–24,26] Depending on the noble metal, the dialkylamine formation may exceed the paraffin formation.[22] The formation of trialkylamines, imines, nitriles and olefins during amine HDN has also been reported, although in smaller quantities than the secondary amine formation.[11,18,22,23]

This study aims to compare the HDN reaction network and kinetics of primary, secondary, and tertiary alkyl amines over the Pt/ZrO_2 catalyst. Furthermore, the goal is to investigate the role of the condensation products in the overall HDN reaction network. Therefore, dodecylamine (C12 amine), didodecylamine (C24 amine), and tridodecylamine (C36 amine) were hydrotreated at 80 bar H_2 over Pt/ZrO_2 at a reaction temperature of 300 °C in a batch reactor. The amines were chosen as model compounds for alkyl amines which are found in bio-based feeds and are also formed as intermediates during hydrotreating of nitrogen containing compounds[5,12,26]. The experimental concentration-time data was used for kinetic modeling with an isothermal power law approach to gain further insight into the reactivity of the model compounds.

Experimental

Materials

For the catalyst preparation platinum(IV) nitrate (15 wt% Pt) from Alfa Aesar was used as metal precursor. For the support, monoclinic zirconia (ZrO_2) from Saint-Gobain Norpro (SZ 31164) was used. The following chemicals were used for the reactor experiments without further purification: Dodecylamine (>99.0 %, Sigma Aldrich), didodecylamine (>97.0 %, Sigma Aldrich), tridodecylamine (>97.0 %, Sigma Aldrich), decalin (decahydronaphthalene, mixture of cis and trans, >99%, Sigma Aldrich), nitrogen (99.999 %, Woikoski), and hydrogen (99.999 %, Woikoski). The same hydrogen gas was also used for the analytics. Furthermore, synthetic air (99.999 %), helium (99.999 %), argon (99.999 %) and oxygen (99.999 %) from Woikoski were used. *n*-Pentadecane (>99%, Sigma Aldrich) was used as an internal standard and propan-2-ol (>99.5 %, Fisher Chemicals) as a second solvent for the GC analytics.

Catalyst preparation

The Pt/ZrO_2 catalyst was synthesized with a vacuum impregnation method according to Verkama et al.[18] The support (ZrO_2) was crushed, sieved (particle size of sieve 0.25-0.45 mm), and calcined for 10 h at 600 °C in a static muffle furnace. For the impregnation, 2.5 g of ZrO_2 was dried in a 100 mL round-bottom flask at 60 °C for 90 min under vacuum in a rotary evaporator. The metal precursor was dissolved in type 1 ultra-pure water with approximately four times the pore volume of

the support. The precursor solution was added to the support at room temperature, under vacuum and stirring. The solution was stirred for 2 h under vacuum, allowing the excess impregnation solution to slowly evaporate and the catalyst precursor was dried the following day under vacuum for 60 min at 40 °C and 30 min at 60 °C. The Pt catalyst was calcined in a flow through calcination oven at 100 ml/min in synthetic air at 450 °C for 1 h with a heating ramp of 2 °C/min.

Catalyst Characterization

Inductively Coupled Plasma Optical Emission Spectroscopy

The Pt content of the catalyst was determined using inductively coupled plasma optical emission spectroscopy (ICP-OES). Prior to the analysis, the catalyst sample was digested in aqua regia using a Speedwave XPERT Microwave Pressure Digestion System (Berghof, Analytic Jena). The sample was then diluted with ultrapure type 1 water, filtered, and analyzed. The ICP-OES analysis was performed using an Agilent 5900 SVDV ICP-OES spectrometer. The Pt 203.646 nm and Pt 214.424 nm lines were analyzed, and Scandium (255.235 nm) was used as an internal standard. For details on the ICP-OES analysis, see the supplementary information.

X-ray Diffraction Analysis

The calcined catalyst was analyzed using X-ray diffraction (XRD) with a PANanalytical X'PERT PRO MPD Alpha1 device, with a PIXcel 1D detector and X-ray source consisting of a Cu monochromator, utilizing K-alpha1 emission with a wavelength of 0.15405980 nm. The analysis range was 5-100 °, with a step size of 0.026 ° and a time per step of 96.36 s. A programmable divergence slit was used, but a mathematical fixed divergence slit correction was performed on the data. Samples were crushed prior to analysis using a mortar and pestle.

CO Pulse Titration

CO pulse titration was done using a Micromeritics AutoChem III device. Approximately 200 mg of catalyst was added to the sample tube. Prior to chemisorption, the catalyst was dried in He flow at 200 °C for 120 min and reduced in 5% H_2/Ar at 350 °C for 120 min. After reduction, the sample was kept at 350 °C in He flow for 45 min, to remove chemisorbed hydrogen, and cooled down to 50 °C. Next, 15 pulses of 10% CO/Ar, each with a volume of 0.5185 ml, were introduced to the sample. The CO consumption was monitored using a thermal conductivity detector and a MKS Instruments Cirrus 3 mass spectrometer, which monitored the signals at m/z = 28 (CO), m/z=44 (CO_2) and m/z=18 (H_2O). The temperature of the loop and the equipment's lines was 110 °C. The dispersion and platinum particle size were calculated based on the CO consumption, assuming hemispherical Pt particles and an adsorption stoichiometry of 1.

N_2 Physisorption

Nitrogen physisorption at 77 K was used to determine the specific surface and the total pore volume of the catalyst. The catalyst was analyzed in both calcined form and reduced form, using the same samples as used for CO chemisorption. The measurement was performed with a Micromeritics Tristar Plus device. Prior to the measurement, the catalyst was degassed at 350 °C in nitrogen flow for 300 min. The specific surface area was determined using Brunauer-Emmett-Teller (BET) method[33] (relative pressure range 0.05-0.25), while the pore size distribution and the total pore volume specific surface area were determined using Barrett-Joyner-Halenda (BJH) method[34].

Carbon Analysis

A Thermo Flash Smart CHNSO Elemental Analyzer was used to determine the amount of carbon present in the spent catalysts. 2,5-Bis(5-tert-butyl-benzoxazol-2-yl)thiophene (BBOT) was used as a calibration standard. The temperature of the (left) furnace was 950°C, the temperature of the oven was 65°C, the carrier gas flow was 140 ml/min, the reference gas flow was 100 ml/min, the oxygen flow was 250 ml/min, the oxygen injection end time was 4s, the sampling delay time was 12 s and the run time was 750 s.

Catalytic Activity tests

For the experiments a 100 mL Hastelloy batch reactor from Parr Instrument Company was used. For the amine HDN experiments, 20 mg of the Pt/ZrO_2 catalyst was dried *in-situ* at 180 °C and 10 bar N_2 for 60 min. The catalyst was then reduced in-situ at 350 °C and 20 bar H_2 for 60 min while stirring with 100 rpm.

The reaction mixture was prepared as a solution of the respective alkyl amine in 27.8 g decalin, targeting a total initial nitrogen concentration of 100 ppm (mg/L). Therefore, the mass of the alkyl amines varied accordingly, with 41.0 mg for the dodecylamine, 78.3 mg for the didodecylamine, and 115.5 mg for the tridodecylamine. The reaction mixture was heated (to approximately 80 °C) under constant stirring to dissolve the amine in the solvent. Before the reaction, 1 mL of the reaction mixture (zero-sample) was taken to quantify the reactants. The reaction mixture was inserted into the pre-heated feed vessel (heater set to 100 °C) and released into the reactor, which had been heated to the reaction temperature of 300 °C. For the reaction, the reactor was pressurized at 80 bar H_2 and the stirring set to 600 rpm, marking the start of the reaction. The reaction time varied between 15 min and 300 min, corresponding to a batch residence time τ of 0-500 $g_{cat}h/mol_{N,\,feed}$. The stirring was stopped, and the reaction was quenched with an ice bath after the reaction time elapsed. Finally, 1 mL of sample (reaction-sample) was taken for analysis.

The 60 min reaction for the dodecylamine was repeated three time as a control experiment. To test for thermal activity of each amine, the procedure was repeated without the catalyst, the drying and reduction, and with a reaction time of 60 min. The activity of the ZrO_2 support activity was tested with the same procedure as for the amine HDN experiments using ZrO_2 instead of the catalyst with a reaction time of 60 min.

Product Analysis

To avoid precipitation of the products and reactants in the 1 mL analysis samples, 0.18 mL propan-2-ol was added as a second solvent before the analysis. As an internal standard (ISTD) 6 μL *n*-pentadecane was also added beforehand.

Qualitative analysis of reaction products

The samples were analyzed with gas chromatography with a mass spectrometer (GC-MS) using Shimadzu's GCMS-QP2010 SE equipped with a HP-5MS column (30 m x 0.250 mm x 0.25 µm) by Agilent J&W GC Columns to identify reactants and products using multiple programs.

Quantification of liquid products

The reaction products were quantified with gas chromatography (GC), using an Agilent Technologies 7890B GC System equipment with a flame ionization detector (FID) and a nitrogen-phosphorus detector (NPD) and using an Agilent J&W HP1-MS column (60 m x 0.25 mm x 0.25 μm). Two GC-FID methods were used for the product quantification, details on these methods can be found in the supplementary information.

For determining the reactant and product concentrations with the FID, the relative response factors (RRF) of dodecylamine, didodecylamine, *n*-dodecane, 1-dodecan-ol and isopropyl-dodecylamine were estimated based on their combustion enthalpy and weight, using a method developed by de Saint Laumer et al.[35,36] For the tridodecylamine, an experimental calibration for the RRF was made, the results can be found in the supplementary information.

The carbon balance closure B_C (%) for each amine HDN experiment was calculated using Equation 1

$$B_{\mathrm{C}} = \frac{c_{\mathrm{C,products}}}{c_{\mathrm{C,feed}}} \cdot 100\% \qquad (1)$$

where $c_{c,products}$ (mmol/L) is the concentration of carbon of the products and $c_{c,feed}$ (mmol/L) is the concentration of carbon of the feed. The carbon balance closures for the experimental data can be found in the supplementary information.

Carbon-based yields Y_C (%) for each of each product species were calculated using Equation 2

$$Y_{\mathrm{C}} = \frac{c_{\mathrm{product}}\, a_{\mathrm{C,product}}}{c_{\mathrm{reactant}}\, a_{\mathrm{C,reactant}}} \cdot 100\% \qquad (2)$$

where a_C is the number of carbon atoms in a compound.

Total Nitrogen Content Analysis

The nitrogen content (ppm) of the samples was measured with a P422022 ElemeNts nitrogen analyzer from PAC L.P. The injection volume for the analysis was 20 µL and each sample was measured three times.

The nitrogen removal N_{removal} (%) was calculated from both the GC-FID and N-Analyzer results using Equation 3

$$N_{\mathrm{removal}} = \left(1 - \frac{\rho_{\mathrm{N,products}}}{\rho_{\mathrm{N,feed}}}\right) \cdot 100\% \qquad (3)$$

where $\rho_{\mathrm{N,products}}$ is the nitrogen content (mg/L) in the reaction sample and $\rho_{\mathrm{N,feed}}$ is the density of nitrogen (mg/L) in the zero sample.

Kinetic Modeling

Kinetic modeling of the amine HDN batch reactions was done using Jupyter Notebook 6.5.4 from Python 3.11. The concentration/time profile of the reactants were mathematically modeled assuming power law kinetics. The optimal set of kinetic parameters was obtained using the *scipy.optimize.least_squares*[37,38] solver. The parameter bounds for all reaction rate constants were set to 0 - 1. Several different initial values for the parameters were tested, with no significant effect on the fitting results.

Results & Discussion

Catalyst Preparation and Characterization

A summary of the catalyst characterization results is shown in Table 1. The data shows that the Pt/ZrO_2 catalyst has the targeted metal loading, the pore volume was 0.25 cm^3/g and the BET surface area was 38.9 m^2/g. The surface area and pore volume of the support did not change significantly during impregnation, calcination, and reduction of the catalyst. Based on the CO chemisorption results, the Pt particle size was 3.8 nm and the dispersion was 29 %. X-ray diffraction showed only the peaks associated with the m-ZrO_2 support (ICDD 00-065-0687) (see the Supplementary Information). This implies no large, XRD-visible Pt crystallites were present, which was well in agreement with the CO chemisorption results. Thus, it appears that the catalyst synthesis was successful, the obtained Pt/ZrO_2 catalyst was well-dispersed and had the correct metal loading.

Table 1. Pore volume, BET surface area, Pt content, Pt particle size and dispersion for the reduced catalyst as well as the m-ZrO_2 support. Pore volume and BET surface area were determined using N_2-physisorption, Pt-content was determined by ICP-OES and the Pt particle size and dispersion were determined using CO pulse chemisorption. The same sample was used for CO chemisorption and N-physisorption. Prior to analysis, this sample was reduced at 350 °C for 120 min in 5% H_2/Ar, as outlined in the "Experimental"-section.

Sample	Pore volume (cm^3/g)	BET surface area (m^2/g)	Pt (wt-%)	Pt particle size (nm)	Dispersion
m-ZrO_2	0.26	38	-	-	-
Pt/ZrO_2	0.25	39	1.0	3.8	29 %

HDN Experiments

Figure 1 shows the composition of the product samples and the nitrogen removals as a function of batch residence time for the primary, secondary, and tertiary amines hydrotreating experiments. The data shows that the Pt/ZrO_2 catalyst is active for the HDN of dodecylamine (C12 amine), didodecylamine (C24 amine), and tridodecylamine (C36 amine). The final product for hydrotreating of all three amines is dodecane (C12 paraffin). The secondary amine appears to be a major intermediate during HDN of both primary and tertiary amine, while primary amine is formed as an intermediate during HDN of secondary amine. Small amounts of the tertiary amine and dodecan-1-ol (C12 alcohol) were also present as intermediates. In addition to these compounds, trace amounts of an acetone-derived side product were detected (N-isopropyldodecan-1-amine). It is proposed to have formed by carbonyl-amine condensation of the dodecylamine and acetone. The acetone was a residue from cleaning the feed vessel and reactor, thus it does not belong to the HDN network of the primary, secondary, and tertiary

alkylamines. The carbon balance closure of all amine HDN experiments over Pt/ZrO2 ranged from 92-105 %, indicating that there were no major unaccounted products.

Based on the data shown in Figure 1, there are clear differences in the reactivity of the primary, secondary, and tertiary amines. The low batch residence time data in Figure 1a-c indicates that the secondary amine is an initial product during both primary amine and tertiary amine hydrotreating. For the secondary amine hydrotreating, less than 5 % of primary amine is present as an intermediate. It is also clear that the secondary amine can be formed in a condensation reaction between two molecules of primary amine, as has been reported before.[22,23,29,39] However, only trace amounts of tertiary amine were detected during the primary and secondary amine experiments. This may indicate that a condensation reaction between the primary and secondary amine is not favored, or that the tertiary amine formed in such a reaction is rapidly converted to other products.

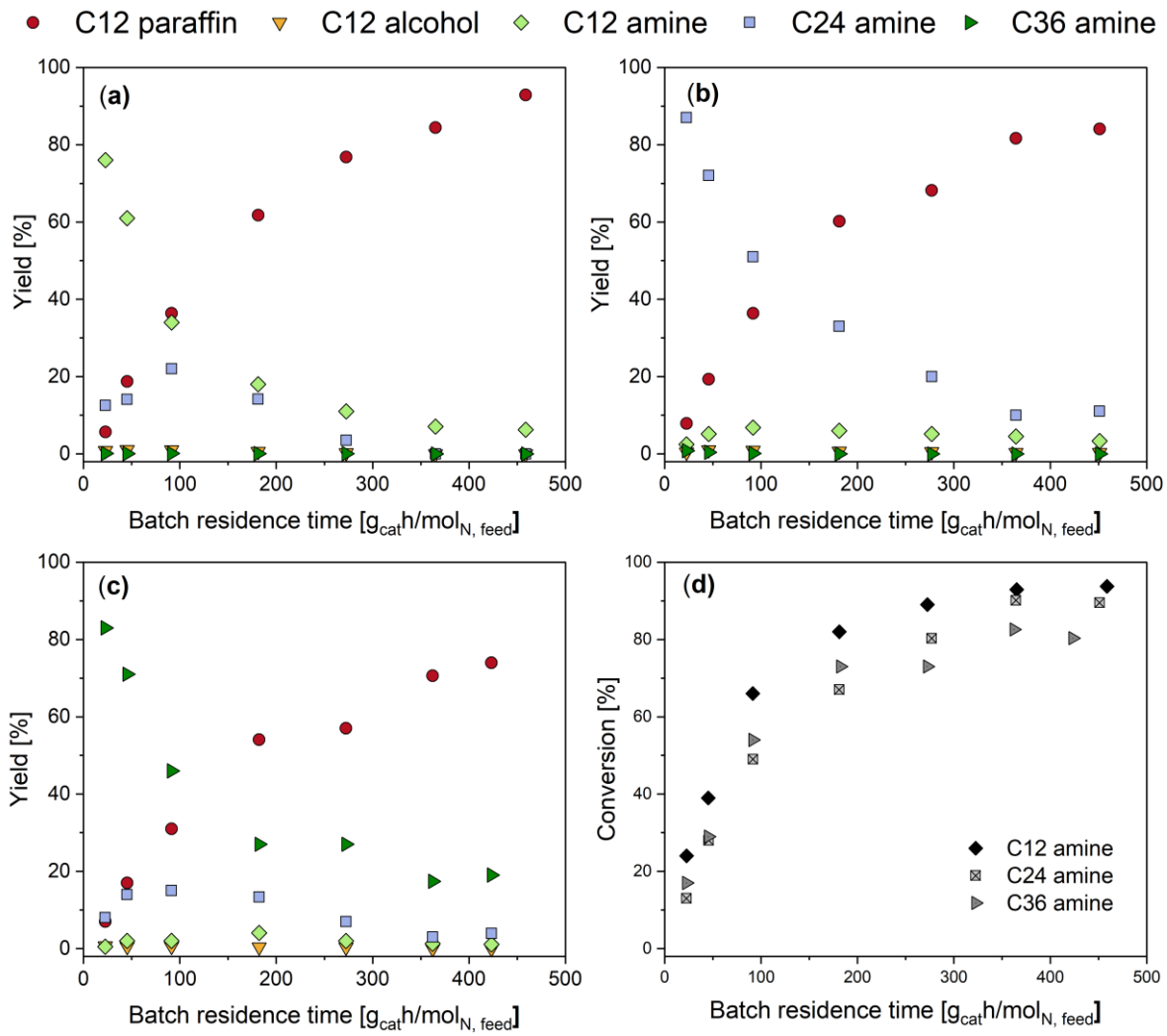

Figure 1. Carbon-based yields as a function of Batch residence time ($g_{cat}h/molN_{,feed}$) for: (a) the dodecylamine HDN experiments, (b) the didodecylamine HDN experiments, (c) tri-dodecylamine HDN experiments, as well as conversion (%) as a function of batch residence time (d). Experimental conditions: 300 °C, 80 bar H_2, 20 mg catalyst and 100 ppm initial nitrogen concentration.

Figure 1 also shows that at higher batch residence times, the conversion rate of the amines slows down, and the intermediates are consumed as dodecane, the final product, is formed. Generally, it appears that amine HDN occurs much slower at higher batch residence times, which can be explained by a lower concentration of reactants. However, deactivation cannot be ruled out based on the experimental data. A CHNS analysis of the spent catalyst showed no evidence for deactivation by coking, as the carbon content of the spent catalyst used in the secondary amine experiments did not appear to increase at higher batch residence times (see the Supplementary Information).

Figure 2 shows nitrogen removal (a) and paraffin yield (b) for the three amines as a function of batch residence time, as well as the paraffin yields as a function of nitrogen removal (c) and nitrogen removals as a function of conversion (d). On one hand, as shown by Figure 1 and Figure 2a, conversion of primary amine is slightly faster than conversion of the tertiary and secondary amines, while the nitrogen removal decreases in the order primary amine > secondary amine > tertiary amine. On the other hand, the paraffin yield is essentially the same for all three amines at batch residence times below 100 $g_{cat}h/mol_{N,feed}$ (see Figure 2b), although at higher batch residence time the tertiary amine has a lower paraffin yield than the secondary and primary amine.

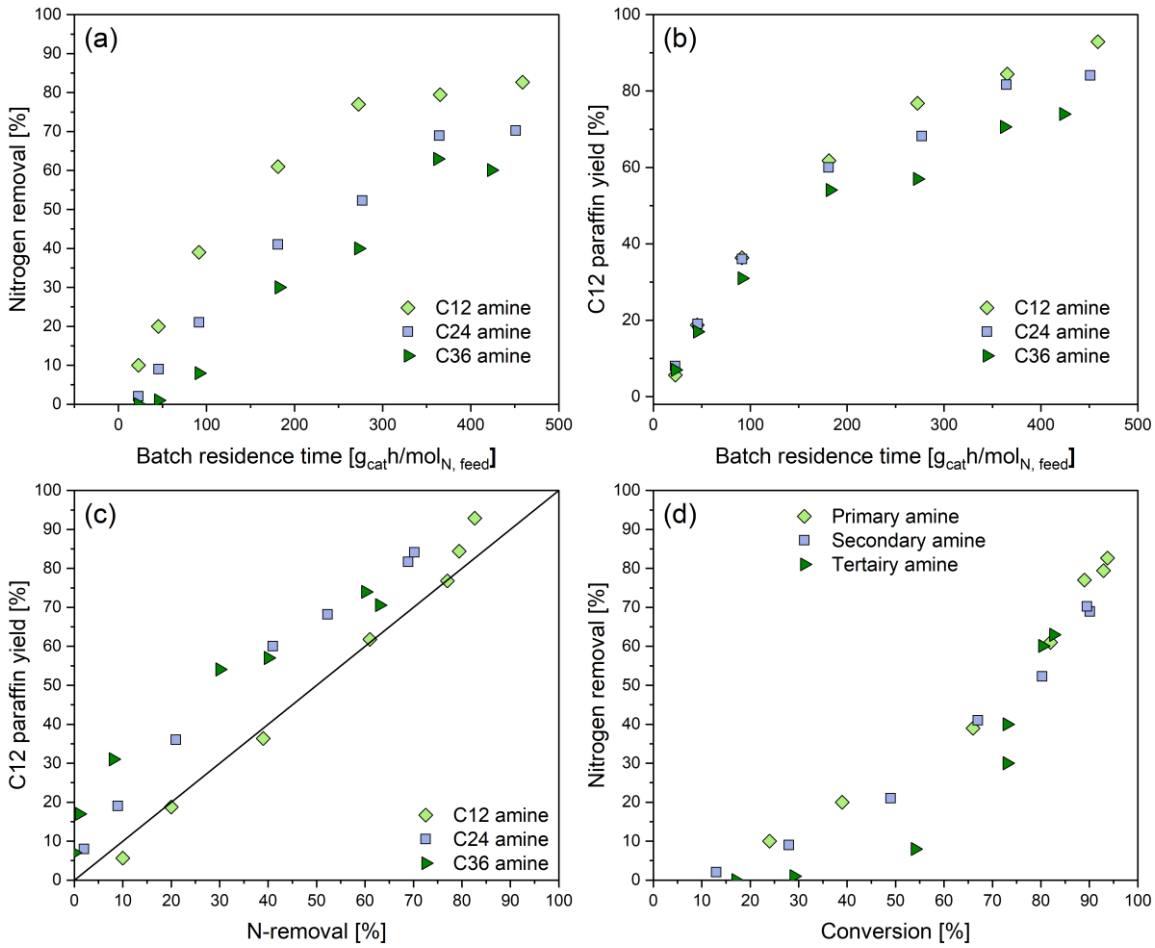

Figure 2. Nitrogen removal (a) and paraffin yield (b) as a function of batch residence time for the experiments with different amines, as well as paraffin yield as a function of nitrogen removal (c) and nitrogen removal as a function of conversion of the respective amines (d). Experimental conditions: 300 °C, 80 bar H_2, 20 mg catalyst and 100 ppm initial nitrogen concentration.

Thus, it appears that for the primary amine, the paraffin is formed concurrently with nitrogen removal, while for both secondary and tertiary amine, paraffin is formed initially, before nitrogen removal takes place. This is supported by Figure 2c, which shows the paraffin yield as a function of the nitrogen removal. For the primary amine, the paraffin yield initially has a linear relationship with the nitrogen removal, showing that both paraffin formation and nitrogen removal initially takes place. However, for secondary and tertiary amine the increase in paraffin yield, as nitrogen removal increases, is steeper, indicating that paraffin is formed before nitrogen removal takes place. Indeed, as shown by Figure 2d, nitrogen removal of the tertiary amine increases slowly as the conversion increases, showing that the initial tertiary amine conversion step does not involve nitrogen removal. Thus, the data presented in Figure 1 and Figure 2 indicates that there are clear differences in how HDN proceeds for the primary, secondary, and tertiary amines.

Based on the data shown in Figure 1, it appears that the primary and secondary amines are always present as intermediates during HDN of primary, secondary, and tertiary amines, while the tertiary amine is not formed in significant amounts. As indicated by the conversion, nitrogen removal and paraffin yield data, HDN is fastest for the primary amine, while the tertiary amine and the secondary amines form paraffins faster than they undergo HDN. Based on these observations, it is deemed likely that the HDN of the tertiary amine occurs through the secondary amine, while the HDN of the secondary amine involves the primary amine as an intermediate. Thus, the reaction network shown in Figure 3 is proposed.

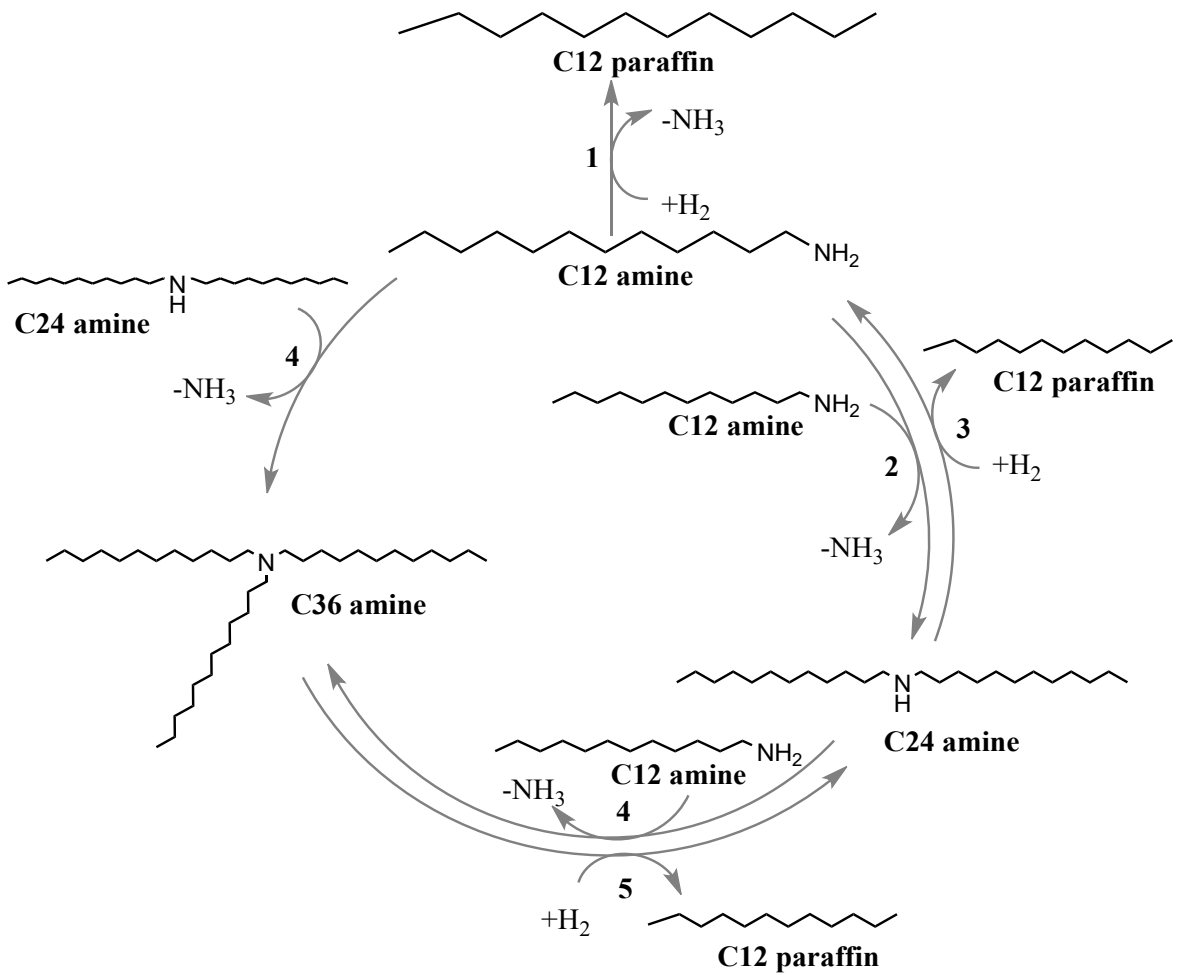

Figure 3. Reaction network for the hydrotreatment of primary amine (dodecylamine, **C12 amine**), secondary amine (didodecylamine, **C24 amine**) and tertiary amine (tridodecylamine, **C36 amine**) over Pt/ZrO_2. The hydrotreatment of all three amines produces dodecane (**C12 paraffin**) as the final product. Reactions: **1** direct HDN of primary amine, **2** condensation of primary amine, **3** hydrogenolysis of secondary amine, **4** condensation of secondary amine, **5** hydrogenolysis of tertiary amine.

In the proposed reaction network (Figure 3), the primary amine can react directly through hydrodenitrogenation (**1**) or undergo a condensation reaction (**2**) to form the secondary amine. The secondary amine decomposes via hydrogenolysis into dodecane and primary amine (**3**). While a condensation reaction between primary amine and secondary amine (**4**) may seem feasible, no evidence for formation of significant amounts of tertiary amine was detected in the primary and secondary amine experiments. This may be due to this condensation reaction not being favored, or due to the tertiary amine decomposing via hydrogenolysis into dodecane and secondary amine (**5**) as quickly as it is formed.

The proposed reaction network shown in Figure 3 is well in line with the observed conversion trend. Conversion of the primary amine can take place through one of two mechanisms: direct HDN (**1**) and condensation (**2**), while conversion of secondary and tertiary amines takes place through a C-N bond hydrogenolysis step. The trend in the nitrogen removal can also be explained: all initial reaction steps for the primary amine (**1, 2, 4**) involve the loss of nitrogen, while nitrogen removal

with the secondary amine first involves formation of the primary amine (**3**), and nitrogen removal with the tertiary amine occurs through secondary amine and primary amine intermediates (**5, 3**). Indeed, nitrogen removal occurs only through the primary amine, either through condensation reactions (**2, 4**) or through direct HDN (**1**).

The proposed reaction network is well in line with previous studies investigating the reactions of amines over noble metals. Condensation reactions between primary amines, forming secondary amines, have long been known to take place in the presence of hydrogen and a metal catalyst. For example, in 1932 Winans and Adkins[39] reported the formation of dipentylamine from pentylamine using nickel catalysts, and in 1986 Meitzner *et al.*[22] studied the reactions of methylamine on Pt/SiO_2, and found that significant amounts of dimethylamine were formed. More recent work by Verkama *et al.*[29,29] confirmed that such condensation reactions also can take place on Pt/ZrO_2 for tetradecylamine and hexadecylamine, which have carbon chain lengths more relevant for industrial HDN. The hydrotreating reactions of secondary and tertiary amines have also been studied by Sivasankar *et al.*[23], who showed that on Pd/Al_2O_3, dipentylamine may undergo hydrogenolysis to form pentylamine and pentane/pentene, as well as also undergo a bimolecular reaction to form primary amine and tertiary amine. In this study, we found that the hydrogenolysis of didodecylamine takes place on Pt/ZrO_2 but found no evidence for a bimolecular reaction between two molecules of didodecylamine. Sivasankar *et al.*[23] also found that *tri*-pentylamine reacted exclusively through hydrogenolysis to dipentylamine and olefin/paraffin[23], which matches well the results obtained in this study for hydrotreating of tridodecylamine.

Kinetic Modeling

Kinetic modeling was carried out with the aim to quantitatively describe the data with a suitable physical kinetic model based on the proposed reaction mechanism. For the kinetic modeling, power law kinetics were assumed. The model assumed constant concentration of hydrogen in the reaction mixture, since hydrogen was present in large excess. The power law model was isothermal and did not consider mass transfer or diffusion limitations. The kinetic modeling was done based on the reaction network shown in Figure 3, and also includes the condensation (**6**) of two molecules of secondary amine to primary amine and tertiary amine as described by Sivasankar *et al*. [23] The reaction rate equations are shown Table 2, the stoichiometric matrix can be found in the supplementary information and the molar amounts changing rates in Table 3.

Table 2. Reaction rates r_j of the HDN reaction network in Figure 3 and secondary amine condensation.

Reaction	Reaction rate equation
Direct hydrodenitrogenation (**1**) of primary amine	$r_1 = k_1 c_{\mathrm{H}} c_{\mathrm{C12A}} = k_1' c_{\mathrm{C12A}}$
Condensation (**2**) two primary amine	$r_2 = k_2 c_{\mathrm{C12A}}^2$
Hydrogenolysis (**3**) of secondary amine	$r_3 = k_3 c_{\mathrm{H}} c_{\mathrm{C24A}} = k_3' c_{\mathrm{C24A}}$
Condensation (**4**) of primary amine and secondary amine	$\mathrm{r}_4 = k_4 c_{\mathrm{C12A}} c_{\mathrm{C24A}}$
Hydrogenolysis (**5**) of tertiary amine	$r_5 = k_5 c_{\mathrm{H}} c_{\mathrm{C36A}} = k_5' c_{\mathrm{C36A}}$
Condensation (**6**) of two secondary amine	$r_6 = k_6 c_{\mathrm{C24A}}^2$

Figure 4 shows the experimentally determined concentrations of the reactants and products, as well as the concentrations predicted by the (optimized) kinetic model. Overall, the model appears to match the experimental data well, although it overestimates the tertiary amine formation during the primary and secondary amine experiments. For further comparison of predictive and experimental values, refer to the parity plots given in the supplementary information. The fitted reaction rate constants are reported in Table 4.

The rate constants for direct HDN of dodecylamine (**1**), hydrogenolysis of didodecylamine (**3**) and hydrogenolysis of tridodecylamine (**5**) shown in Table 4 have similar values (0.012-0.016 min^{-1}). This is reasonable, since all three reactions involve the cleavage of a C-N bond. The reaction rate constant for the reaction between two didodecylamine molecules is practically zero, and we thus have not found any evidence that this reaction takes place for didodecylamine on Pt/ZrO_2. Thus, our decision to not include it in the reaction network in Figure 3 appears justified.

Table 3. Molar amount changing rates R_i for primary amine (C12 A), secondary amine (C24 A), tertiary amine (C36 A), and dodecane (C12 P).

R_{C12A} =	$-1r_1 - 2r_2 + 1r_3 - 1r_4 + 0r_5 + r_6 =$	$-k_1' c_{\mathrm{C12A}} - 2k_2 c_{\mathrm{C12A}}^2 + k_3' c_{\mathrm{C24A}} - k_4 c_{\mathrm{C12A}} c_{\mathrm{C24A}} + k_6 c_{\mathrm{C24A}}^2$
R_{C24A} =	$0r_1 + 1r_2 - 1r_3 - 1r_4 + 1r_5, -2r_6 =$	$k_2 c_{\mathrm{C12A}}^2 - k_3' c_{\mathrm{C24A}} - k_4 c_{\mathrm{C12A}} c_{\mathrm{C24A}} + k_5' c_{\mathrm{C36A}} - 2k_6 c_{\mathrm{C24A}}^2$
R_{C12P} =	$1r_1 + 0r_2 + 1r_3 + 0r_4 + 1r_5 =$	$k_1' c_{\mathrm{C12A}} + k_3' c_{\mathrm{C24A}} + k_5' c_{\mathrm{C36A}}$
R_{C36A} =	$0\mathrm{r}_1 + 0\mathrm{r}_2 + 0\mathrm{r}_3 + 1\mathrm{r}_4 - 1\mathrm{r}_5 + 1\mathrm{r}_6 =$	$\mathrm{k}_4 \mathrm{c}_{\mathrm{C12A}} \mathrm{c}_{\mathrm{C24A}} - k_5' c_{\mathrm{C36A}} + k_6 c_{\mathrm{C24A}}^2$

The reaction rate constants were used to calculate the reaction rates r_1-r_6 and the nitrogen removal rate, using the rate equations in Table 1. The predicted nitrogen removal rate in was calculated as a sum of all reaction rates involving nitrogen removal, namely, r_1, r_2, r_4 and r_6. These rates, the nitrogen removal predicted by the kinetic model and the experimental nitrogen removal (GC-FID based) are plotted in Figure 5.

As can be seen in Figure 5a, in the primary amine experiments, nitrogen removal starts immediately and slows down at longer reaction times. The direct HDN (**1, r_1**) and the condensation (**2, r_2**) of two primary amines make up most of the overall nitrogen removal for the primary amine experiment, with r_1 (direct HDN) being the fastest. The simulated nitrogen removal rate for the secondary and tertiary amine experiment goes through a maximum at 30 min for the secondary amine and 100 min for the tertiary amine. As the primary amine is formed through secondary amine hydrogenolysis, the nitrogen removal rate increases, but when the primary amine is later decomposed, the nitrogen removal rate decreases again. In other words, the nitrogen removal rate correlates with the concentration of the primary amine, which indicates that the primary amine is involved in all nitrogen removal pathways. This is further supported by the nitrogen removal rate maximum occurring at longer reaction times for the tertiary amine, which first forms the secondary amine and then the primary amine. Even though

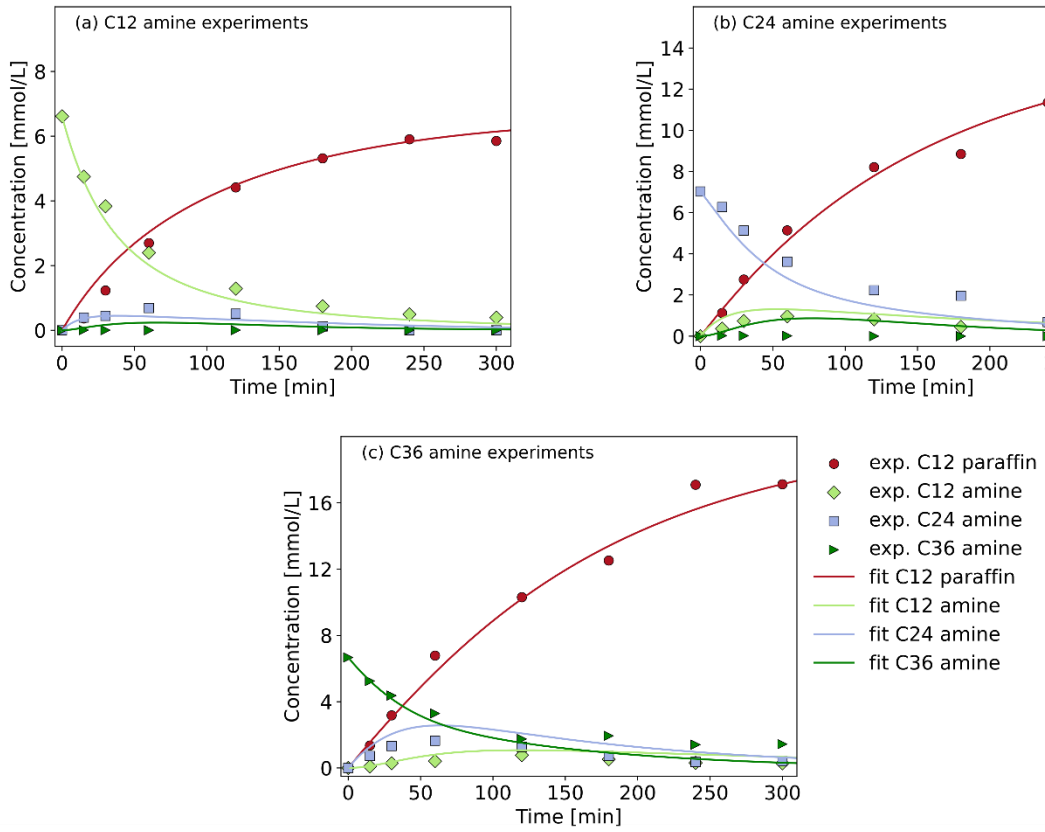

Figure 4. Experimental (exp.) data and simulated fit as concentration (mmol/L) vs. reaction time (min) for (a) the primary amine experiments, (b) the secondary amine experiments, and (c) the tridodecylamine experiments. Experimental conditions: 300 °C, 80 bar H_2, 20 mg catalyst and 100 ppm initial nitrogen concentration.

the tertiary amine is equally reactive as the secondary amine in terms of conversion (see Figure 1d) the maximum nitrogen removal rate of the secondary amine comes sooner.

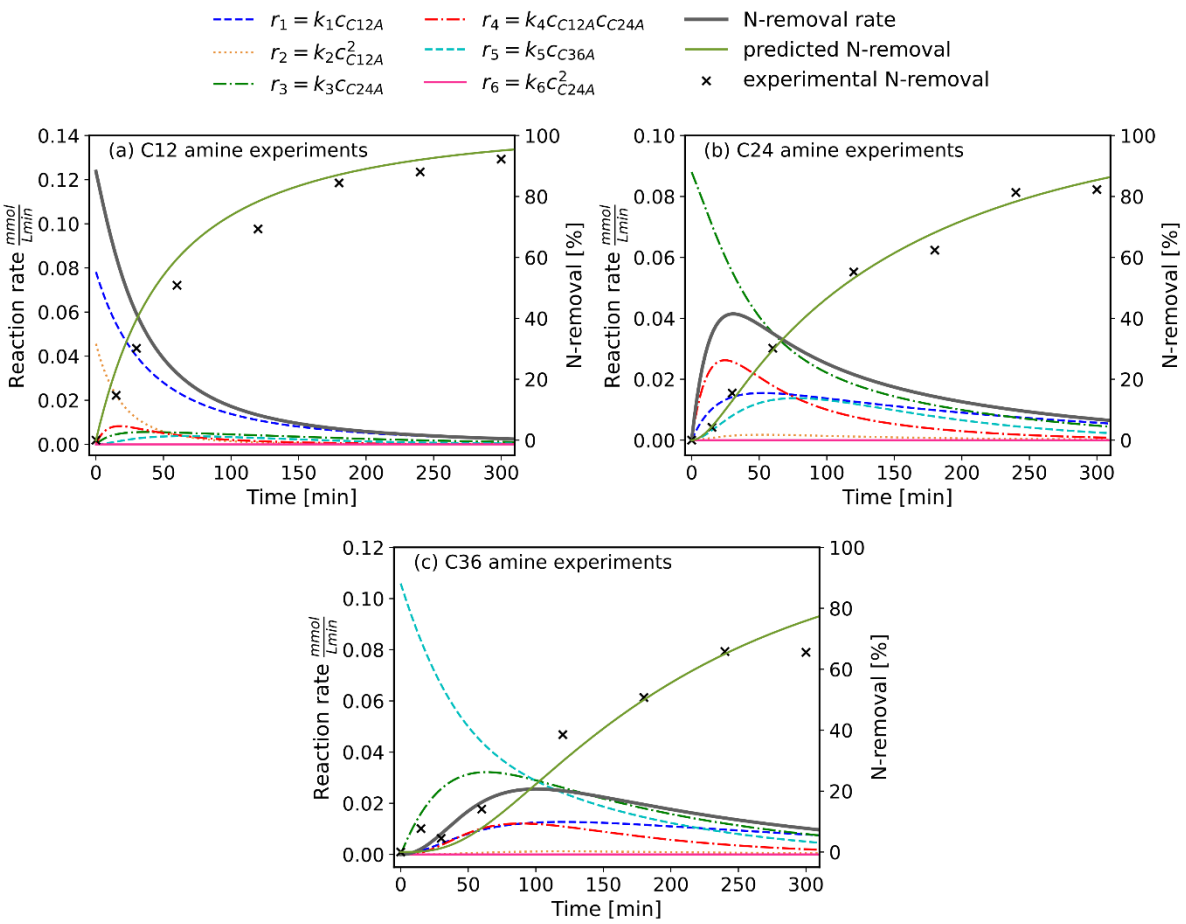

Figure 5. On the left axis reaction rates and nitrogen removal rate (mmol/Lmin) and on the right axis experimental nitrogen removal (%) (from the GC-FID/NPD, including the nitrogen from the acetone derived side product) and simulated nitrogen removal (%) vs reaction time [min] for the (a) dodecylamine HDN experiments, (b) didodecylamine HDN experiments, and (c) the tridodecylamine experiments. Experimental conditions: 300 °C, 80 bar H_2, 20 mg catalyst and 100 ppm initial nitrogen concentration.

Table 4. Reactions of the amine HDN reaction network in Figure 3 and their simulated reaction rate constants k_i. Modeling conditions: Power Law model, least squares solver, including reaction rate r_4.

Reactions	**Fitted reaction rate constants**	
Direct hydrodenitrogenation (**1**) of primary amine	k_1' (1/min)	0.012
Condensation (**2**) of two primary amines	k_2 (L/mmol·min)	0.001
Hydrogenolysis (**3**) of secondary amine	k_3' (1/min)	0.013
Condensation (**4**) of primary amine and secondary amine	k_4 (L/mmol·min)	0.005
Hydrogenolysis (**5**) of tertiary amine	k_5' (1/min)	0.016
Condensation (**6**) of two secondary amines	k_6 (L/mmol· min)	10^{-12}

Effect of the condensation reactions on amine HDN

As discussed in Section 3.2, the formation of significant amounts of tridodecylamine was not detected during the primary and secondary amine experiments. However, the modeling results indicate that the condensation reaction (**4**) between primary and secondary amine, forming tertiary amine, appears to significantly contribute to the nitrogen removal in the secondary and tertiary amine experiments. It should be noted that the experimental concentration of the tridodecylamine was very low in the primary and secondary amine experiments, and that the GC-FID based tertiary amine concentrations thus likely have large uncertainties associated with them. The amount of tertiary amine formed in the secondary and primary amine experiments was also overestimated by the kinetic model. Therefore, to check the fitting results related to this condensation reaction (**4**), a fit without this reaction was done (r_4 was set to zero). These results can be found in the supplementary information. Without the condensation reaction between primary and secondary amine, the dodecylamine concentration was underestimated by the model in the primary amine experiments and overestimated in the secondary amine experiments. Furthermore, the nitrogen removal in the secondary and tertiary amine experiments was underestimated, indicating that the condensation (**4**) does play a role in the overall nitrogen removal, even though this was not apparent from the raw experimental data. This would furthermore show the overall importance of the condensation reactions in the amine HDN reaction network.

The low amount of tertiary amine detected in the liquid phase may be due to the tertiary amine forming in higher concentrations in the catalyst pore system, but, because of diffusion limitations, being unable to leave the pores before it reacts further via hydrogenolysis (**5**). It should be noted that due to its size, pore diffusion of the tertiary amine is expected to be slower than that of the primary and secondary amines. This may also be why the reaction (**6**) involving two molecules of secondary amine does not take place for didodecylamine on Pt/ZrO_2. We hypothesize that this reaction cannot take place inside the catalyst pore structure due to steric hindrance, which prevents two molecules of secondary amine from approaching each other inside the pores. It is noteworthy that the primary amine is involved in both condensation reactions we have found evidence for; either two molecules of primary amine react, or one molecule of primary amine and one molecule of secondary amine react. We thus suspect that mass transfer limitations involving the larger secondary and tertiary amines could play a significant role during amine hydrotreating. By choosing the correct pore size distribution for the catalyst, it may even be feasible to develop shape-selective HDN catalysts, which suppress the formation of condensation products from long-chained primary amines.

The effect of the condensation reaction pathways (**2**, **4**) on the overall amine HDN rate can be deduced from the data and the proposed reaction network. Initially, nitrogen removal of primary amine can take place both through direct HDN (**1**) and through condensation (**2**). As seen in Figure 1a, at low batch residence times the condensation reaction pathway is significant

and secondary amine is formed faster than it decomposes. Based on the kinetic modeling results shown in Figure 5, the rate of condensation reaction (**2**) is approximately half of the rate of primary amine direct HDN (**1**). In this condensation reaction, two molecules of primary amine are consumed, and one molecule of ammonia formed. This thus explains why conversion and nitrogen removal of the primary amine is faster than that of the secondary and tertiary amine (see Figure 1d and Figure 2a).

However, the secondary amine formed in the condensation reaction cannot undergo direct HDN, but instead undergoes hydrogenolysis to reform one molecule of the primary amine. The condensation reaction thus momentarily consumes two molecules of primary amine, but only liberates one molecule of ammonia. The other N-atom is "trapped" in the secondary amine intermediate, until this intermediate decomposes to form primary amine, which can undergo HDN. As the kinetic data in Table 4 shows that C-N bond splitting steps have similar rate constants for primary and secondary amines, nitrogen removal in two steps (through the condensation pathway) is overall slower than nitrogen removal through direct HDN. Thus, we propose that the condensation reactions increase the initial nitrogen removal rate, but that at higher reaction times the condensation reactions instead may start slowing down overall HDN as part of the nitrogen is present as secondary and tertiary amine. To highlight this effect of the condensation reactions on primary amine HDN, we compared the results calculated using the kinetic parameters fitted to the experimental data with the results calculated using the same parameters, but without any condensation reactions taking place (k_2, k_4, k_6 set to zero). The results are shown in the supplementary information and are well in agreement with the above discussion. The nitrogen removal initially increases faster for the model which includes the condensation reactions, but at high reaction times nitrogen removal is slightly higher for the model for which condensation reactions do not take place.

Conclusions

In this study, the HDN of primary, secondary, and tertiary alkyl amines, namely dodecylamine, didodecylamine, and tridodecylamine, over a Pt/ZrO_2 catalyst was examined. Based on the results, all three amines were found to share the same reaction network. The nitrogen removal increased in the order primary amine > secondary amine > tertiary amine. This is well in agreement with the proposed reaction network, in which the initial reactions of the secondary and tertiary amine mainly involved hydrogenolysis into paraffin as well as primary and secondary amine, respectively. Indeed, all steps involving nitrogen removal involve the primary amine, which can either undergo direct HDN through hydrogenolysis, or undergo a condensation reaction with another molecule of primary or secondary amine. The kinetic modeling results showed that the reaction rate constants for the hydrogenolysis reactions of the primary, secondary, and tertiary amines were similar, which is not unexpected since all three reactions involve the C-N bond hydrogenolysis of a saturated amine.

This study thus emphasizes the connection of the reaction networks of primary, secondary, and tertiary alkyl amines in the HDN over a noble metal catalyst (Pt/ZrO_2). While the model compounds share a reaction network, the conversion and nitrogen removal considerably depend on the reactant, as the initial reaction pathways varied accordingly. As the HDN of secondary and tertiary amines was found to be slower than HDN of primary amines, HDN of feedstock containing more highly substituted amines is likely to be more difficult. We also suggest that condensation reactions involving primary amines initially increased nitrogen removal, but at longer reaction times may slightly decrease nitrogen removal, as nitrogen is present in the form of secondary and tertiary amines, which cannot undergo direct HDN. This has implications for both catalyst and process design for HDN of feeds containing primary aliphatic amines. If a lower degree of nitrogen removal is acceptable, it may be beneficial to develop catalysts or processes which promote the formation of condensation products since these reactions contribute to nitrogen removal at low reaction times. However, if a high degree of nitrogen removal is required, the formation of condensation products may need to be avoided.

Conflicts of interest

The authors declare no conflict of interest.

Data availability

The data supporting this article have been included as part of the Supplementary Information.

Author contributions

E.V. prepared the catalyst and developed the batch reactor experiment methodology. The reactor experiments were planned by E.V., L.F.K, R.K. and R.L.P. Batch reactor experiments and analysis of the reaction products was carried out by L.F.K., J.K. and E.V. Catalyst characterization was performed by J.K., E.V. and J.V. The kinetic modeling was performed by L.F.K., supervised by L.I. and M.R. The first version of the manuscript was written by J.K. and L.F.K. All authors contributed to the final version of the manuscript.

Acknowledgements

We thank Sylvia Albersberger and all other members of the Neste-Aalto HDN catalyst development project group for useful discussions and insights. The experimental work for this study was funded by Neste Corporation (Neste-Aalto HDN catalyst development project). J.K. also acknowledges The Finnish Foundation for Technology Promotion for additional funding during the writing process. The Bioeconomy and Raw materials research infrastructures at Aalto University were used for the experimental work in this study. This work was done in collaboration between researchers at Aalto University and Technische Universität Darmstadt. This collaboration was carried out within the UNITE! University Network for Innovation, Technology and Engineering.

References

(1) Bergero, C.; Gosnell, G.; Gielen, D.; Kang, S.; Bazilian, M.; Davis, S. J. Pathways to Net-Zero Emissions from Aviation. *Nat. Sustain.* **2023**, *6* (4), 404–414. https://doi.org/10.1038/s41893-022-01046-9.

(2) International Air Transport Association. Developing Sustainable Aviation Fuel, 2022. https://www.iata.org/en/programs/environment/sustainable-aviation-fuels/, retrieved 10.09.2024.

(3) ReFuelAviation Initiative: Sustainable Avaiation Fuels and the 'fit for 55'package, 2022. https://www.europarl.europa.eu/thinktank/en/document/EPRS_BRI(2022)698900, retrieved 10.09.2024.

(4) Klöwer, M.; Allen, M. R.; Lee, D. S.; Proud, S. R.; Gallagher, L.; Skowron, A. Quantifying Aviation's Contribution to Global Warming. *Environ. Res. Lett.* **2021**, *16* (10), 104027. https://doi.org/10.1088/1748-9326/ac286e.

(5) Furimsky, E. Hydroprocessing Challenges in Biofuels Production. *Catal. Today* **2013**, *217*, 13–56. https://doi.org/10.1016/j.cattod.2012.11.008.

(6) Cavani, F.; Albonetti, S.; Basile, F.; Gandini, A. *Chemicals and Fuels from Bio-Based Building Blocks*; Wiley-VCH Verlag GmbH & Co. KGaA: Weinheim, Germany, 2016. https://doi.org/10.1002/9783527698202.

(7) Neste MY Renewable Diesel Lowers Your CO2 Emissions. https://www.neste.us/neste-my-renewable-diesel, retrieved 10.09.2024.

(8) Ecofining. https://www.eni.com/en-IT/actions/energy-transition-technologies/biofuels/biomass-ecofining.html, retrieved 10.09.2024.

(9) Furimsky, E. Catalytic Hydrodeoxygenation. *Appl. Catal. Gen.* **2000**, *199* (2), 147–190. https://doi.org/10.1016/S0926-860X(99)00555-4.

(10) Gutiérrez-Antonio, C.; Gómez-Castro, F. I.; de Lira-Flores, J. A.; Hernández, S. A Review on the Production Processes of Renewable Jet Fuel. *Renew. Sustain. Energy Rev.* **2017**, *79*, 709–729. https://doi.org/10.1016/j.rser.2017.05.108.

(11) Furimsky, E.; Massoth, F. E. Hydrodenitrogenation of Petroleum. *Catal. Rev.* **2005**, *47* (3), 297–489. https://doi.org/10.1081/CR-200057492.

(12) Chen, W.-T.; Tang, L.; Qian, W.; Scheppe, K.; Nair, K.; Wu, Z.; Gai, C.; Zhang, P.; Zhang, Y. Extract Nitrogen-Containing Compounds in Biocrude Oil Converted from Wet Biowaste via Hydrothermal Liquefaction. *ACS Sustain. Chem. Eng.* **2016**, *4* (4), 2182–2190. https://doi.org/10.1021/acssuschemeng.5b01645.

(13) Leng, L.; Zhang, W.; Peng, H.; Li, H.; Jiang, S.; Huang, H. Nitrogen in Bio-Oil Produced from Hydrothermal Liquefaction of Biomass: A Review. *Chem. Eng. J.* **2020**, *401*, 126030. https://doi.org/10.1016/j.cej.2020.126030.

(14) Prado, G. H. C.; Rao, Y.; de Klerk, A. Nitrogen Removal from Oil: A Review. *Energy Fuels* **2017**, *31* (1), 14–36. https://doi.org/10.1021/acs.energyfuels.6b02779.

(15) Huber, G. W.; O'Connor, P.; Corma, A. Processing Biomass in Conventional Oil Refineries: Production of High Quality Diesel by Hydrotreating Vegetable Oils in Heavy Vacuum Oil Mixtures. *Appl. Catal. Gen.* **2007**, *329*, 120–129. https://doi.org/10.1016/j.apcata.2007.07.002.

(16) Mortensen, P. M.; Grunwaldt, J.-D.; Jensen, P. A.; Knudsen, K. G.; Jensen, A. D. A Review of Catalytic Upgrading of Bio-Oil to Engine Fuels. *Appl. Catal. Gen.* **2011**, *407* (1–2), 1–19. https://doi.org/10.1016/j.apcata.2011.08.046.

(17) Bu, Q.; Lei, H.; Zacher, A. H.; Wang, L.; Ren, S.; Liang, J.; Wei, Y.; Liu, Y.; Tang, J.; Zhang, Q.; Ruan, R. A Review of Catalytic Hydrodeoxygenation of Lignin-Derived Phenols from Biomass Pyrolysis. *Bioresour. Technol.* **2012**, *124*, 470–477. https://doi.org/10.1016/j.biortech.2012.08.089.

(18) Verkama, E.; Auvinen, P.; Albersberger, S.; Tiitta, M.; Karinen, R.; Puurunen, R. L. Competitive Hydrodeoxygenation and Hydrodenitrogenation Reactions in the Hydrotreatment of Fatty Acid and Amine Mixtures. *Top. Catal.* **2023**. https://doi.org/10.1007/s11244-023-01784-w.

(19) Badari, A. C.; Harnos, Sz.; Lónyi, F.; Onyestyák, Gy.; Štolcová, M.; Kaszonyi, A.; Valyon, J. A Study of the Selective Catalytic Hydroconversion of Biomass-Derived Pyrolysis or Fermentation Liquids Using Propylamine and Acetic Acid as Model Reactants. *Catal. Commun.* **2015**, *58*, 1–5. https://doi.org/10.1016/j.catcom.2014.07.041.

(20) Palardy, O.; Behnke, C.; Laurens, L. M. L. Fatty Amide Determination in Neutral Molecular Fractions of Green Crude Hydrothermal Liquefaction Oils From Algal Biomass. *Energy Fuels* **2017**, *31* (8), 8275–8282. https://doi.org/10.1021/acs.energyfuels.7b01175.

(21) Zhu, C.; Gutiérrez, O. Y.; Santosa, D. M.; Flake, M.; Weindl, R.; Kutnyakov, I.; Shi, H.; Wang, H. Kinetics of Nitrogen-, Oxygen- and Sulfur-Containing Compounds Hydrotreating during Co-Processing of Bio-Crude with Petroleum Stream. *Appl. Catal. B Environ.* **2022**, *307*, 121197. https://doi.org/10.1016/j.apcatb.2022.121197.

(22) Meitzner, G.; Mykytka, W. J.; Sinfelt, H. Metal-Catalyzed Reactions of Methylamine in the Presence of Hydrogen. *J. Catal.* **1986**, No. 98, 513–521.

(23) Sivasankar, N.; PRINS, R. Reactions of Mixed Dialkyl- and Trialkylamines over Pd/\textgreekg-Al2O3. *J. Catal.* **2006**, *241* (2), 342–355. https://doi.org/10.1016/j.jcat.2006.04.032.

(24) Di, L.; Yao, S.; Li, M.; Wu, G.; Dai, W.; Wang, G.; Li, L.; Guan, N. Selective Catalytic Hydrogenolysis of Carbon–Carbon \textgreeks Bonds in Primary Aliphatic Alcohols over Supported Metals. *ACS Catal.* **2015**, *5* (12), 7199–7207. https://doi.org/10.1021/acscatal.5b02180.

(25) Cattenot, M.; Portefaix, J.-L.; Afonso, J.; Breysse, M.; Lacroix, M.; Perot, G. Mechanism of Carbon–Nitrogen Bond Scission on Unsupported Transition Metal Sulfides. *J. Catal.* **1998**, *173* (2), 366–373. https://doi.org/10.1006/jcat.1997.1929.

(26) Verkama, E.; Albersberger, S.; Arandia, A.; Meinander, K.; Tiitta, M.; Karinen, R.; Puurunen, R. L. Hydrodeoxygenation and Hydrodenitrogenation of *n* -Hexadecanamide over Pt Catalysts: Effect of the Support. *Catal. Sci. Technol.* **2024**, *14* (2), 431–448. https://doi.org/10.1039/D3CY01480K.
(27) Snåre, M.; Kubičková, I.; Mäki-Arvela, P.; Eränen, K.; Murzin, D. Yu. Heterogeneous Catalytic Deoxygenation of Stearic Acid for Production of Biodiesel. *Ind. Eng. Chem. Res.* **2006**, *45* (16), 5708–5715. https://doi.org/10.1021/ie060334i.
(28) Cheah, K. W.; Yusup, S.; Loy, A. C. M.; How, B. S.; Skoulou, V.; Taylor, M. J. Recent Advances in the Catalytic Deoxygenation of Plant Oils and Prototypical Fatty Acid Models Compounds: Catalysis, Process, and Kinetics. *Mol. Catal.* **2022**, *523*, 111469. https://doi.org/10.1016/j.mcat.2021.111469.
(29) Verkama, E.; Albersberger, S.; Meinander, K.; Tiitta, M.; Karinen, R.; Puurunen, R. L. Zirconia-Supported Pt, Pd, Rh, Ru, and Ni Catalysts in the Hydrotreatment of Fatty Amides and Amines. *Energy Fuels* **2024**, *38* (5), 4464–4479. https://doi.org/10.1021/acs.energyfuels.3c04372.
(30) Verkama, E.; Järvinen, E.; Albersberger, S.; Meinander, K.; Jiang, H.; Tiitta, M.; Karinen, R.; Puurunen, R. L. Hydrodeoxygenation and Hydrodenitrogenation of N-Hexadecanamide to n-Paraffins: Bimetallic Catalysts Supported on Ceria-Zirconia. *Appl. Catal. Gen.* **2024**, *676*, 119602. https://doi.org/10.1016/j.apcata.2024.119602.
(31) Marafi, M.; Furimsky, E. Hydroprocessing Catalysts Containing Noble Metals: Deactivation, Regeneration, Metals Reclamation, and Environment and Safety. *Energy Fuels* **2017**, *31* (6), 5711–5750. https://doi.org/10.1021/acs.energyfuels.7b00471.
(32) Robinson, A. M.; Hensley, J. E.; Medlin, J. W. Bifunctional Catalysts for Upgrading of Biomass-Derived Oxygenates: A Review. *ACS Catal.* **2016**, *6* (8), 5026–5043. https://doi.org/10.1021/acscatal.6b00923.
(33) Brunauer, S.; Emmett, P. H.; Teller, E. Adsorption of Gases in Multimolecular Layers. *J. Am. Chem. Soc.* **1938**, *60* (2), 309–319. https://doi.org/10.1021/ja01269a023.
(34) Lippens, B. C.; Linsen, B. G.; Boer, J. H. de. Studies on Pore Systems in Catalysts I. The Adsorption of Nitrogen; Apparatus and Calculation. *J. Catal.* **1964**, *3* (1), 32–37. https://doi.org/10.1016/0021-9517(64)90089-2.
(35) de Saint Laumer, J.-Y.; Leocata, S.; Tissot, E.; Baroux, L.; Kampf, D. M.; Merle, P.; Boschung, A.; Seyfried, M.; Chaintreau, A. Prediction of Response Factors for Gas Chromatography with Flame Ionization Detection: Algorithm Improvement, Extension to Silylated Compounds, and Application to the Quantification of Metabolites. *J. Sep. Sci.* **2015**, *38* (18), 3209–3217. https://doi.org/10.1002/jssc.201500106.
(36) de Saint Laumer, J.-Y.; Cicchetti, E.; Merle, P.; Egger, J.; Chaintreau, A. Quantification in Gas Chromatography: Prediction of Flame Ionization Detector Response Factors from Combustion Enthalpies and Molecular Structures. *Anal. Chem.* **2010**, *82* (15), 6457–6462. https://doi.org/10.1021/ac1006574.
(37) Branch, M. A.; Coleman, T. F.; Li, Y. A Subspace, Interior, and Conjugate Gradient Method for Large-Scale Bound-Constrained Minimization Problems. *SIAM J. Sci. Comput.* **1999**, *21* (1), 1–23. https://doi.org/10.1137/S1064827595289108.
(38) Virtanen, P.; Gommers, R.; Oliphant, T. E.; Haberland, M.; Reddy, T.; Cournapeau, D.; Burovski, E.; Peterson, P.; Weckesser, W.; Bright, J.; Van Der Walt, S. J.; Brett, M.; Wilson, J.; Millman, K. J.; Mayorov, N.; Nelson, A. R. J.; Jones, E.; Kern, R.; Larson, E.; Carey, C. J.; Polat, İ.; Feng, Y.; Moore, E. W.; VanderPlas, J.; Laxalde, D.; Perktold, J.; Cimrman, R.; Henriksen, I.; Quintero, E. A.; Harris, C. R.; Archibald, A. M.; Ribeiro, A. H.; Pedregosa, F.; Van Mulbregt, P.; SciPy 1.0 Contributors; Vijaykumar, A.; Bardelli, A. P.; Rothberg, A.; Hilboll, A.; Kloeckner, A.; Scopatz, A.; Lee, A.; Rokem, A.; Woods, C. N.; Fulton, C.; Masson, C.; Häggström, C.; Fitzgerald, C.; Nicholson, D. A.; Hagen, D. R.; Pasechnik, D. V.; Olivetti, E.; Martin, E.; Wieser, E.; Silva, F.; Lenders, F.; Wilhelm, F.; Young, G.; Price, G. A.; Ingold, G.-L.; Allen, G. E.; Lee, G. R.; Audren, H.; Probst, I.; Dietrich, J. P.; Silterra, J.; Webber, J. T.; Slavič, J.; Nothman, J.; Buchner, J.; Kulick, J.; Schönberger, J. L.; De Miranda Cardoso, J. V.; Reimer, J.; Harrington, J.; Rodríguez, J. L. C.; Nunez-Iglesias, J.; Kuczynski, J.; Tritz, K.; Thoma, M.; Newville, M.; Kümmerer, M.; Bolingbroke, M.; Tartre, M.; Pak, M.; Smith, N. J.; Nowaczyk, N.; Shebanov, N.; Pavlyk, O.; Brodtkorb, P. A.; Lee, P.; McGibbon, R. T.; Feldbauer, R.; Lewis, S.; Tygier, S.; Sievert, S.; Vigna, S.; Peterson, S.; More, S.; Pudlik, T.; Oshima, T.; Pingel, T. J.; Robitaille, T. P.; Spura, T.; Jones, T. R.; Cera, T.; Leslie, T.; Zito, T.; Krauss, T.; Upadhyay, U.; Halchenko, Y. O.; Vázquez-Baeza, Y. SciPy 1.0: Fundamental Algorithms for Scientific Computing in Python. *Nat. Methods* **2020**, *17* (3), 261–272. https://doi.org/10.1038/s41592-019-0686-2.
(39) Winans, C. F.; Adkins, H. THE ALKYLATION OF AMINES AS CATALYZED BY NICKEL. *J. Am. Chem. Soc.* **1932**, *54* (1), 306–312. https://doi.org/10.1021/ja01340a046.

Supplementary information for "Catalytic hydrodenitrogenation of primary, secondary, and tertiary C12-alkyl amines over a platinum on zirconia catalyst"

Leoni-Franziska Klingelhöfer[a,b], Joakim Kattelus*[a], Emma Verkama[a,c], Jorge Velasco[a], Leonhard Iser[b], Marcus Rose[b], Reetta Karinen[a], Riikka L. Puurunen[a]

[a.] *Aalto University, School of Chemical Engineering.*
[b.] *Technische Universität Darmstadt, Department of Chemistry.*
[c.] *Present address for E.Verkama: Fraunhofer Institute for Solar Energy Systems ISE, Heidenhofstr. 2, 79110 Freiburg, Germany*

1. Details on the ICP-OES analysis

Approximately 100 mg of catalyst was first digested in aqua regia (7.5 ml HCl and 2.5 ml HNO_3) for 50 min at 200 °C, using a Speedwave XPERT Microwave Pressure Digestion System (Berghof, Analytic Jena). The liquid was then diluted with ultrapure (type 1) water, filtered and analyzed.

The ICP-OES analysis was performed using an Agilent 5900 SVDV ICP-OES spectrometer. The device was equipped with a CCD array detector (167 nm - 785 nm). The loop volume was 3.5 ml and the spray chamber was rinsed 30 times between measurements. The pump speed was set to 12 rpm and the rinse time was 15 s. The liquid sample was introduced by a AVS 6/7 autosampler system, with a uptake pump rate of 23 ml/min, an injection pump rate of 2 ml/min, a valve uptake delay of 26.4 s, a bubble injection time of 1.8 s and a preemptive rinse time of 2.4 s. The Pt 203.646 nm and Pt 214.424 nm lines were analyzed. Scandium (255.235 nm) was used as an internal standard, and the Scandium reference solution was automatically injected using the AVS 6/7 autosampler system.

An Agilent Seaspray borosilicate glass nebulizer was used for liquid sample introduction, together with a borosilicate glass spray chamber and an ICP quartz torch intended for analysis of aqueous samples. The plasma was analyzed in axial mode, with a read time of 10 s, a stabilization time of 10 s and the RF power set to 1.10 kW. The nebulizer flow was 0.70 L/min, the plasma flow 12.0 l/min, the auxiliary flow 1.00 L/min and the make-up flow 0.00 L/min. Four replicate measurements were collected per sample injection, and the results of these replicates were averaged. Two blank 5% HNO_3 samples were analyzed between each sample, to ensure no sample carryover occurred.

2. Details on the GC-FID analysis

Two methods were used for the product quantification, method 1 for the dodecylamine and *di*-dodecylamine HDN experiments and method 2 for the HDN experiments with the heavier *tri*-dodecylamine. For method 1 the injection volume was 2 µL and the inlet split ratio was 5:1, the temperature of the inlet was 325°C. The FID and NPD detector temperatures were 325°C. The program started at 80 °C with a hold time of 3 min. Then the temperature was increased to 100 °C with a ramp of 20 °C/min and was held for 3 min. Next, the temperature was raised to 160 °C with a ramp of 10 °C/min. The final temperature of 325 °C was reached with a ramp of 20 °C/min and held for 20 min. For method 2 the injection volume was 1 µL and the split ratio was 15:1, the temperature of the inlet was 325°C. The temperature of the FID and NPD detectors was 325°C. The program started at 100 °C. Then the temperature was raised to 110 °C with a ramp of 30 °C/min and held for 3 min. Next, the temperature went to 160 °C with a ramp of 20 °C/min. The final temperature of 325 °C was reached with a ramp of 30 °C/min and held for 15 min.

3. Experimental data

Table S1: Experimental data of the HDN of dodecylamine over Pt/ZrO_2. Experimental conditions: 300 °C, 80 bar H_2, 20 mg catalyst and 100 ppm initial nitrogen concentration.

Reaction time	[min]	15	30	60	60	60	120	180	240	300
Batch residence time	[$g_{cat}h/n_{N.reactant}$]	22.8	45.3	91.5	90.9	90.6	181.3	272.6	365.3	458.9
c(reactant), initial	[mmol/L]	6.26	6.28	6.70	6.96	6.79	6.94	6.92	6.99	6.30
c(dodecane)	[mmol/L]	0.37	1.23	2.45	3.01	2.66	4.42	5.31	5.90	5.85
c(dodecylamine)	[mmol/L]	4.75	3.83	2.55	2.58	2.04	1.29	0.74	0.49	0.39
c(dodecane-1-ol)	[mmol/L]	0.06	0.07	0.07	0.07	0.08	0.05	0.02	0.00	0.00
c(N-isopropyldodecane-1-amine + N-dodecylpropan-2-imine)	[mmol/L]	0.50	0.34	0.14	0.14	0.78	0.22	0.16	0.30	0.12
c(di-dodecylamine)	[mmol/L]	0.39	0.45	0.73	0.68	0.65	0.51	0.12	0.00	0.00
c(*tri*-dodecylamine)	[mmol/L]	0.00	0.00	0.00	0.00	0.00	0.00	0.00	0.00	0.00
Conversion	[%]	26	40	63	65	70	83	90	94	93
Nitrogen removal	[%]	10	20	39	44	38	61	77	79	83
Carbon balance closure	[%]	100	101	100	103	99	98	93	96	101

Table S2: Experimental data of the HDN of *di*-dodecylamine over Pt/ZrO_2. Experimental conditions: 300 °C, 80 bar H_2, 20 mg catalyst and 100 ppm initial nitrogen concentration.

Reaction time	[min]	15	30	60	120	180	240	300
Batch residence time	[$g_{cat}h/n_{N.reactant}$]	22.7	45.8	91.7	181.1	277.1	364.5	451.1
c(reactant), initial	[mmol/L]	7.20	7.11	7.03	6.82	7.10	6.93	7.33
c(dodecane)	[mmol/L]	1.12	2.75	5.14	8.21	9.70	11.34	12.34
c(dodecylamine)	[mmol/L]	0.37	0.74	0.97	0.82	0.74	0.63	0.49
c(dodecane-1-ol)	[mmol/L]	0.06	0.15	0.00	0.09	0.08	0.05	0.05
c(N-isopropyldodecane-1-amine + N-dodecylpropan-2-imine)	[mmol/L]	0.07	0.05	0.31	0.10	0.23	0.00	0.00
c(di-dodecylamine)	[mmol/L]	6.27	5.13	3.62	2.23	1.40	0.69	0.75
c(*tri*-dodecylamine)	[mmol/L]	0.02	0.02	0.01	0.00	0.00	0.00	0.00
Conversion	[%]	13	28	49	67	80	90	90
Nitrogen removal	[%]	2	9	21	41	52	69	70
Carbon balance closure	[%]	99	100	98	101	94	97	92

Table S3: Experimental data of the HDN of *tri*-dodecylamine over Pt/ZrO_2. Experimental conditions: 300 °C, 80 bar H_2, 20 mg catalyst and 100 ppm initial nitrogen concentration.

Reaction time	[min]	15	30	60	120	180	240	300
Batch residence time	[$g_{cat}h/n_{N.reactant}$]	22.6	45.3	91.3	182.3	272.5	362.3	423.3
c(reactant), initial	[mmol/L]	6.30	6.19	7.19	6.36	7.30	8.07	7.31
c(dodecane)	[mmol/L]	1.35	3.17	6.78	10.31	12.52	17.09	17.12
c(dodecylamine)	[mmol/L]	0.09	0.28	0.41	0.77	0.52	0.31	0.29
c(dodecane-1-ol)	[mmol/L]	0.13	0.10	0.12	0.08	0.08	0.00	0.08
c(N-isopropyldodecane-1-amine + N-dodecylpropan-2-imine)	[mmol/L]	0.09	0.39	0.38	0.31	0.10	0.20	0.17
c(di-dodecylamine)	[mmol/L]	0.72	1.33	1.64	1.27	0.72	0.36	0.41
c(*tri*-dodecylamine)	[mmol/L]	5.25	4.37	3.29	1.75	1.94	1.41	1.44
Conversion	[%]	17	29	54	73	73	82	80
Nitrogen removal	[%]	0	1	8	30	40	63	60
Carbon balance closure	[%]	100	104	96	100	94	93	104

Table S4: Experimental data of the HDN of dodecylamine, *di*-dodecylamine, and *tri*-dodecylamine (without a catalyst, thermal activity) at 60 min reaction time. Experimental conditions: 300 °C, 80 bar H_2, 100 ppm initial nitrogen concentration.

Reactant	-	dodecylamine	*di*-dodecylamine	*tri*-dodecylamine
c(reactant), initial	[mmol/L]	6.67	7.07	7.71
c(dodecane)	[mmol/L]	0.00	0.19	0.00
c(dodecylamine)	[mmol/L]	6.37	0.00	0.00
c(dodecane-1-ol)	[mmol/L]	0.00	0.00	0.00
c(N-isopropyldodecane-1-amine + N-dodecylpropan-2-imine)	[mmol/L]	0.00	0.00	0.04
c(di-dodecylamine)	[mmol/L]	0.00	6.65	0.26
c(*tri*-dodecylamine)	[mmol/L]	0.00	0.00	7.78
Conversion	[%]	5	6	-1
Nitrogen removal	[%]	-2	-3	0
Carbon balance closure	[%]	95	94	103

Table S5: Experimental data of the HDN of dodecylamine, *di*-dodecylamine, and *tri*-dodecylamine over ZrO_2 60 min reaction time. Experimental conditions: 300 °C, 80 bar H_2, 20 mg ZrO_2 and 100 ppm initial nitrogen concentration.

Reactant	-	dodecylamine	*di*-dodecylamine	*tri*-dodecylamine
Batch residence time	[$g_{cat}h/n_{N.reactant}$]	91.3	91.2	92.2
c(reactant), initial	[mmol/L]	6.79	7.59	6.37
c(dodecane)	[mmol/L]	0.02	0.00	0.00
c(dodecylamine)	[mmol/L]	5.52	0.00	0.00
c(dodecane-1-ol)	[mmol/L]	0.02	0.00	0.00
c(N-isopropyldodecane-1-amine + N-dodecylpropan-2-imine)	[mmol/L]	0.66	0.00	0.00
c(di-dodecylamine)	[mmol/L]	0.08	6.78	0.33
c(*tri*-dodecylamine)	[mmol/L]	0.00	0.05	6.80
Conversion	[%]	19	11	-7
Nitrogen removal	[%]	4	-2	-2
Carbon balance closure	[%]	89	90	103

4. X-ray driffraction results

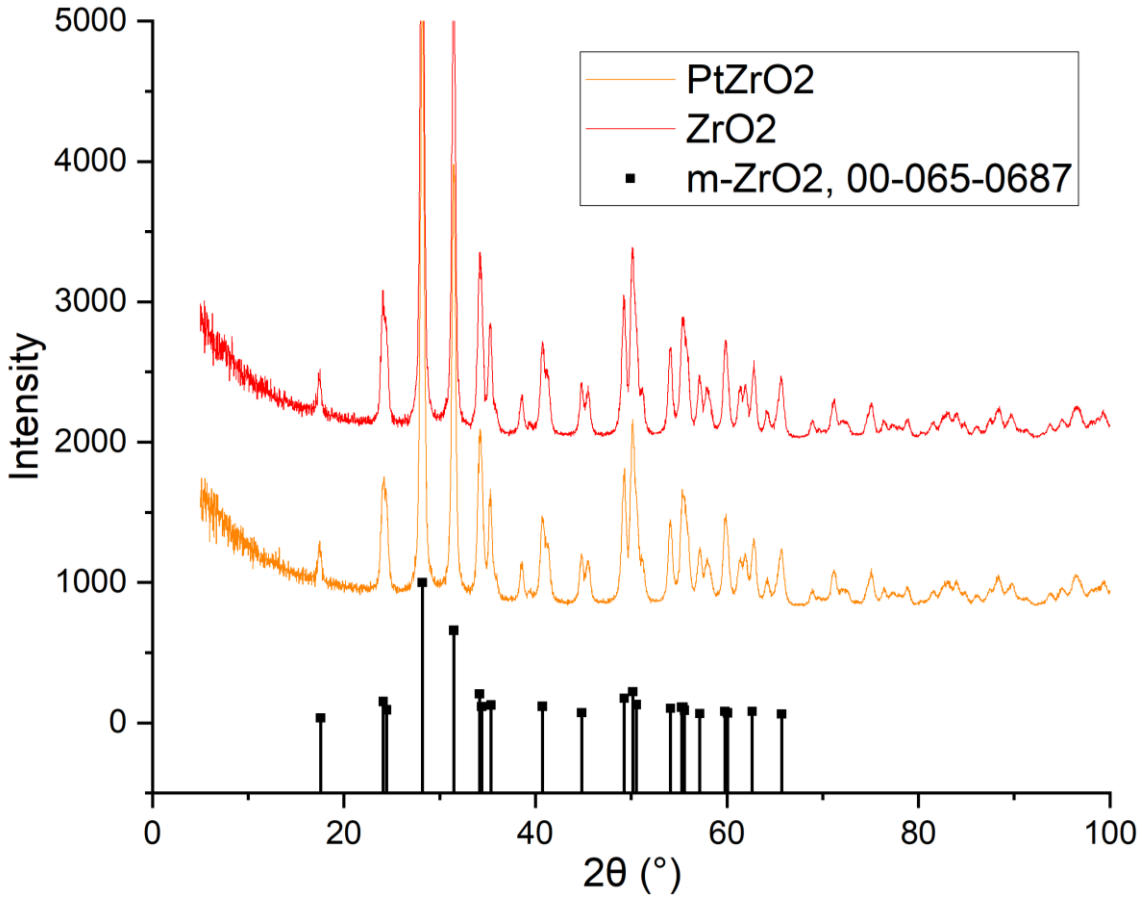

Figure S1. X-ray diffractograms of ZrO_2 and Pt/ZrO_2 as well as the m-ZrO_2 database reference (ICDD 00-065-0687)

5. Kinetic Simulation Supplementary information

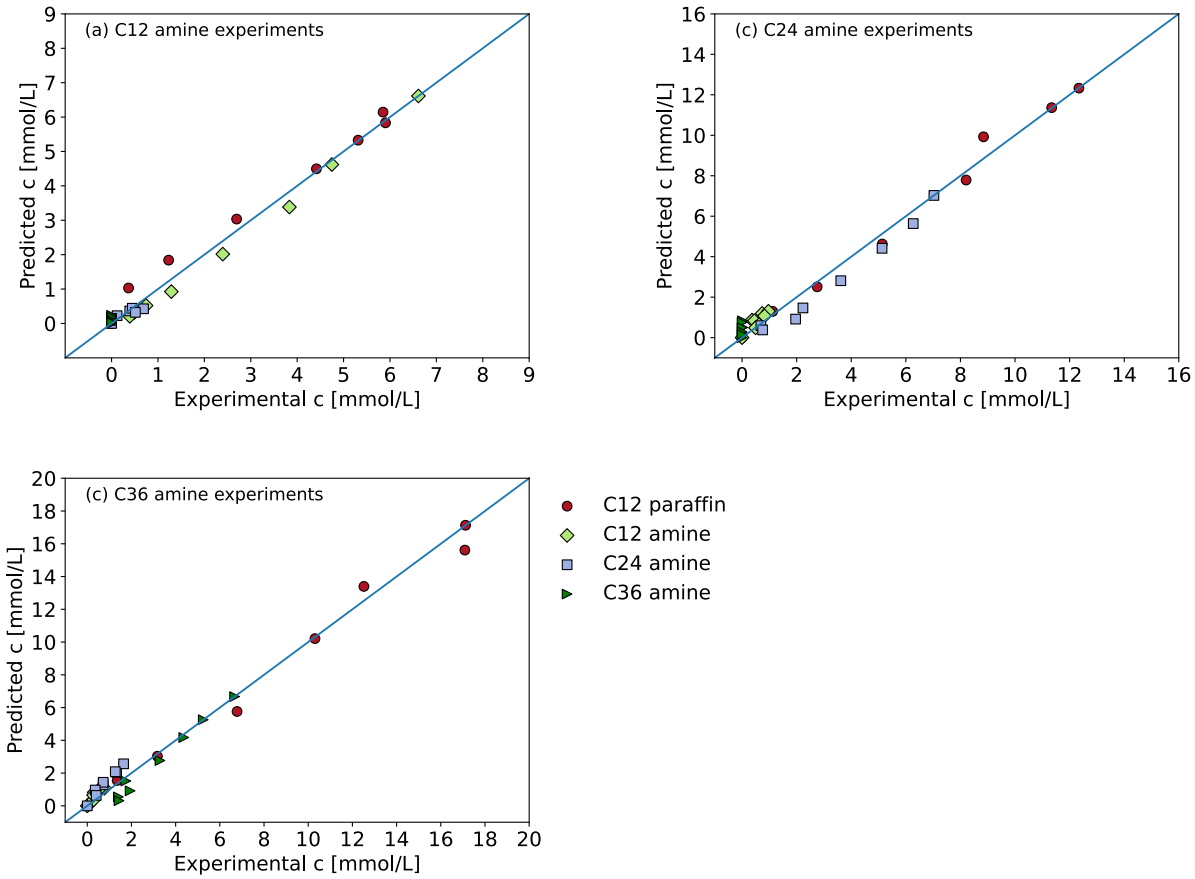

Figure S2: Parity plot with the predicted concentration [mmol/L] vs the experimental concentration [mmol/L] for (a) the dodecylamine experiments, (b) the *di*-dodecylamine experiments, and (c) the *tri*-dodecylamine experiments. Experimental conditions: 300 °C, 80 bar H_2, 20 mg catalyst and 100 ppm initial nitrogen concentration. Modeling conditions: Power Law model, *least squares* solver, including reaction rate r_4.

Table S6 Reactions of the HDN reaction network and their simulated reaction constants k_i. Simulation conditions: Power Law model, *least squares* solver, without reaction rate r_4.

Reactions	Simulated reaction constants	
HDN (**1**)	k_1 [mmol/L min]	0.012691
Condensation (**2**)	k_2 [mmol^2 /L^2 min]	0.002110
Hydrogenolysis (**3**)	k_3 [mmol/L min]	0.012452
Hydrogenolysis (**5**)	k_5 [mmol/L min]	0.013987

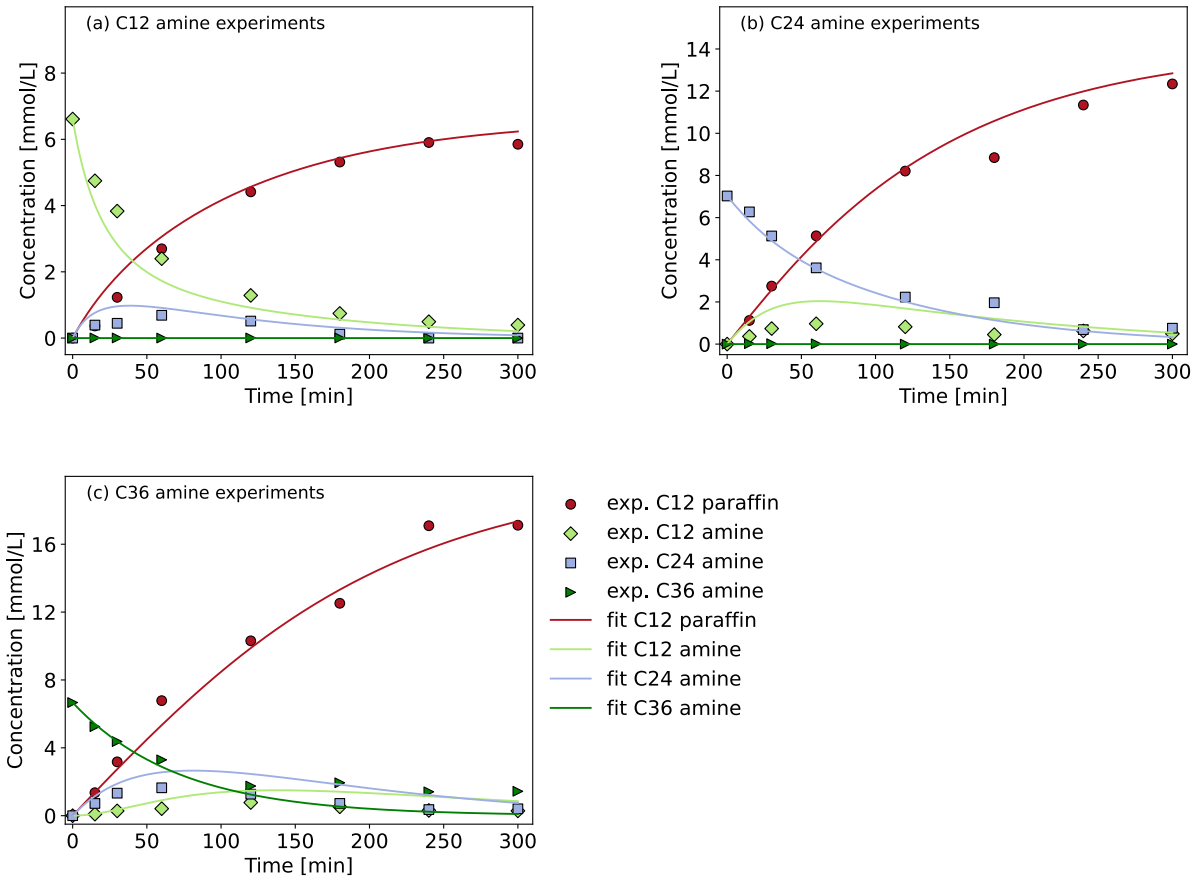

Figure S3: Experimental (exp.) data and simulated fit as concentration [mmol/L] vs. reaction time [min] for (a) the dodecylamine experiments, (b) the *di*-dodecylamine experiments, and (c) the *tri*-dodecylamine experiments. Experimental conditions: 300 °C, 80 bar H_2, 20 mg catalyst and 100 ppm initial nitrogen concentration. Simulation conditions: Power Law model, *least squares* solver, without reaction rate r_4.

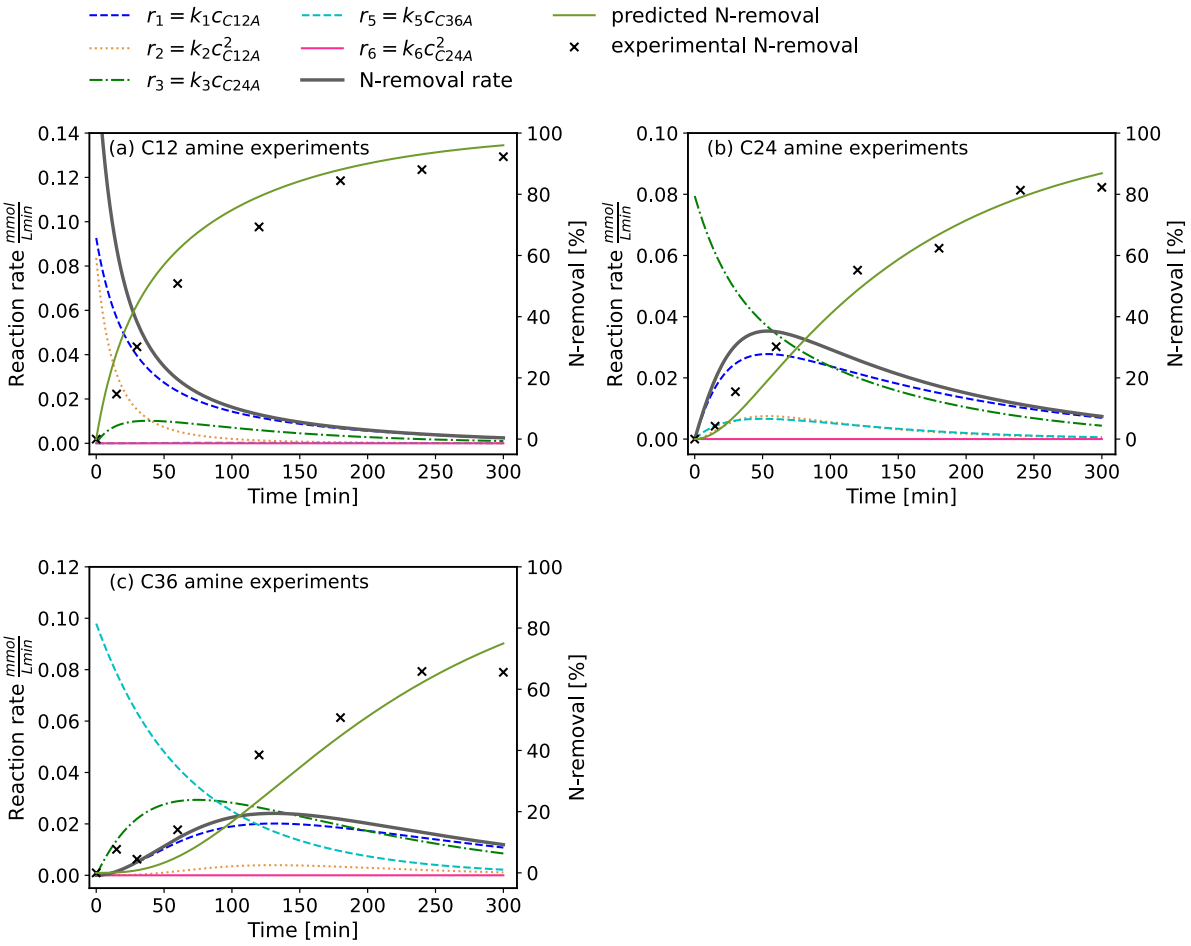

Figure S4: On the right axis reaction rates r_1, r_2, r_3, r_5, r_6 and nitrogen removal rate [mmol/Lmin] vs reaction time [min] and on the left axis experimental nitrogen removal [%] (from the GC-FID/NPD) and simulated nitrogen removal [%] for the (a) dodecylamine HDN experiments, (b) *di*-dodecylamine HDN experiments, and (c) the *tri*-dodecylamine experiments. Experimental conditions: 300 °C, 80 bar H_2, 20 mg catalyst and 100 ppm initial nitrogen concentration. Simulation conditions: Power Law model, *least squares* solver, without reaction rate r_4.

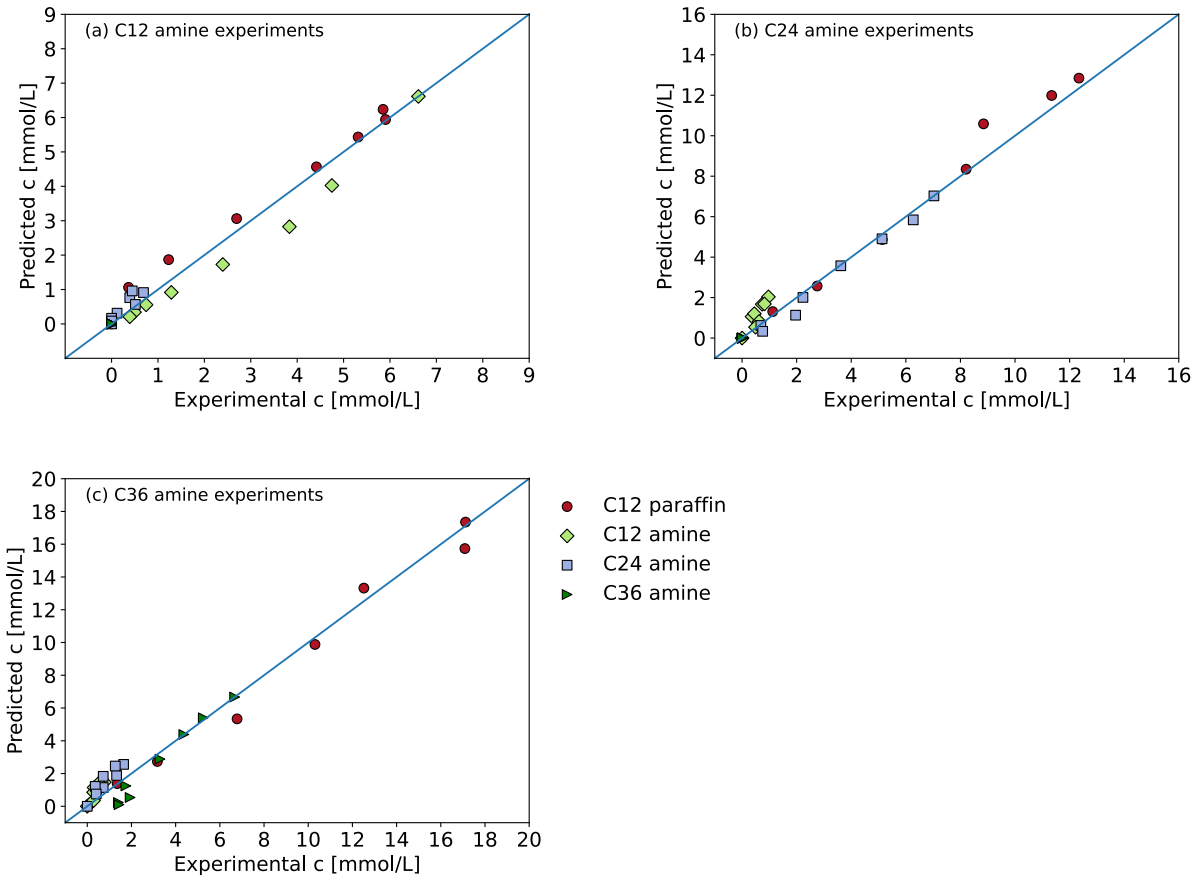

Figure S5: Parity plot with the predicted concentration [mmol/L] vs the experimental concentration [mmol/L] for (a) the dodecylamine experiments, (b) the *di*-dodecylamine experiments, and (c) the *tri*-dodecylamine experiments. Experimental conditions: 300 °C, 80 bar H_2, 20 mg catalyst and 100 ppm initial nitrogen concentration. Simulation conditions: Power Law model, *least squares* solver, without reaction rate r_4.

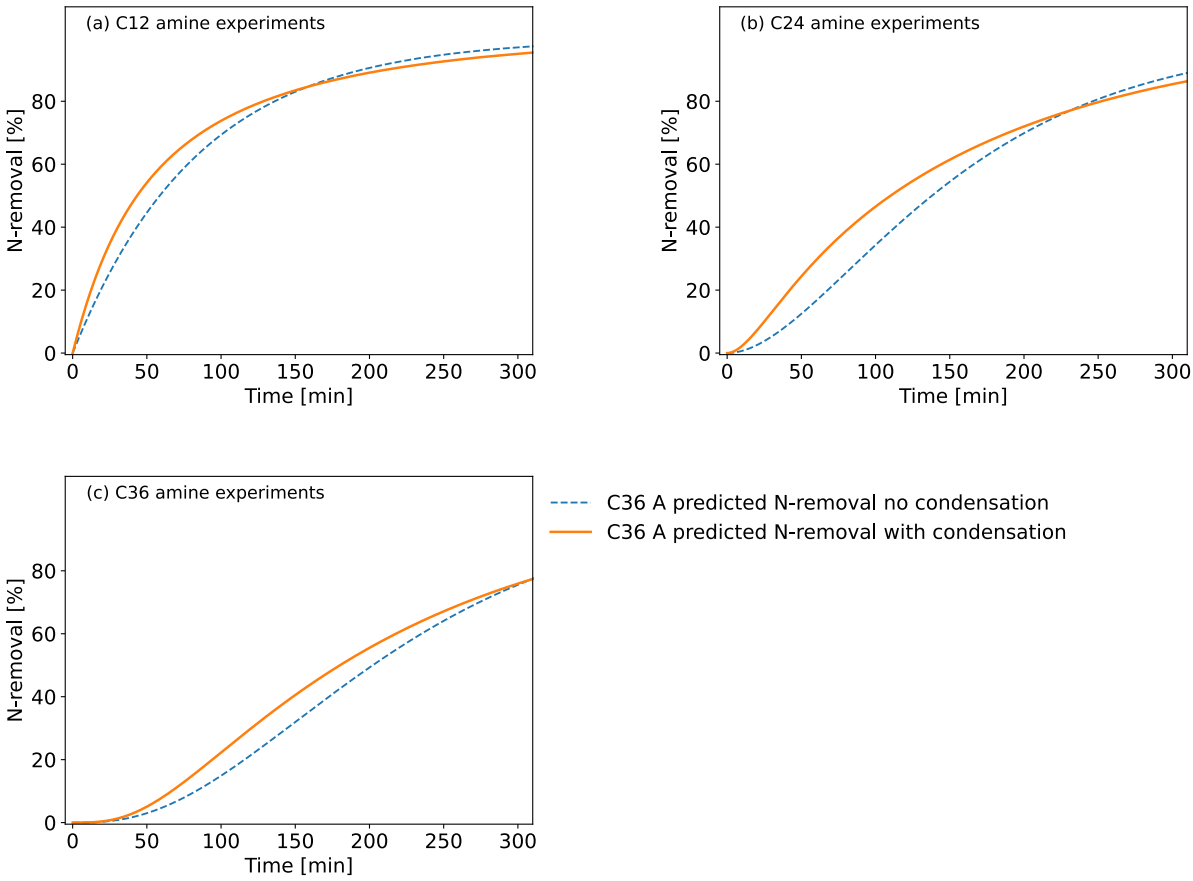

Figure S6: Predicted nitrogen removal with and without the condensation reactions (**2**,**4**,**6**) [%] vs time for (a) the dodecylamine experiments, (b) the *di*-dodecylamine experiments, and (c) the *tri*-dodecylamine experiments. Experimental conditions: 300 °C, 80 bar H_2, 20 mg catalyst and 100 ppm initial nitrogen concentration. Simulation conditions: Power Law model, *least squares* solver.

6. Tridodecylamine calibration curve

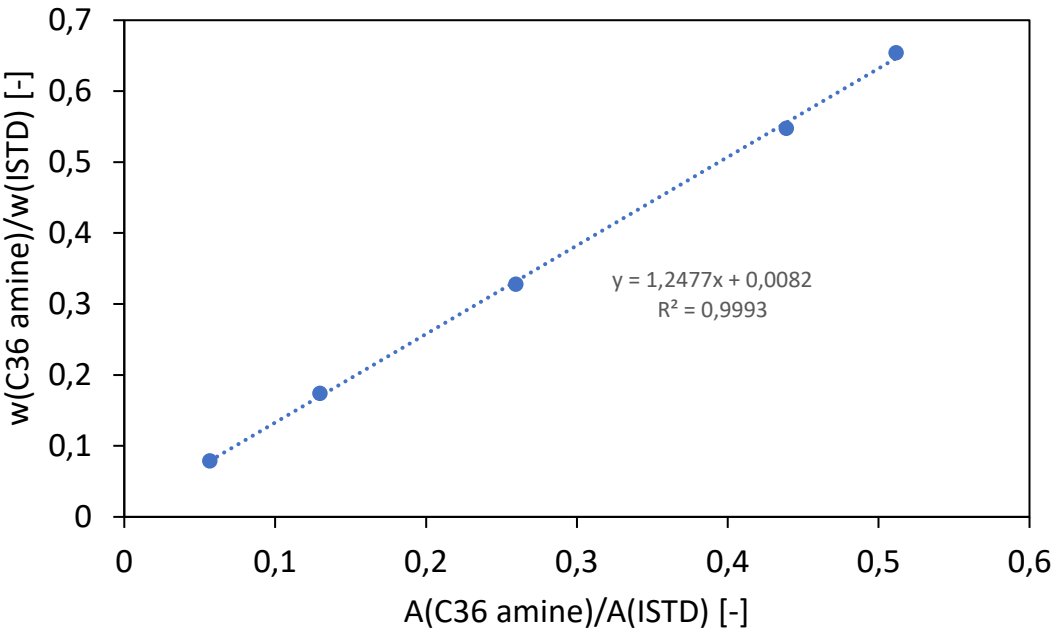

Figure S7: GC-FID calibration curve for tridodecylamine, showing the relationship between the amine peak area, divided by the internal standard peak are, and the amine weight fraction, divided by the internal standard weight fraction. The slope of the line is the relative response factor (RRF).

7. CHNS analysis of the spent catalyst from the secondary amine experiments

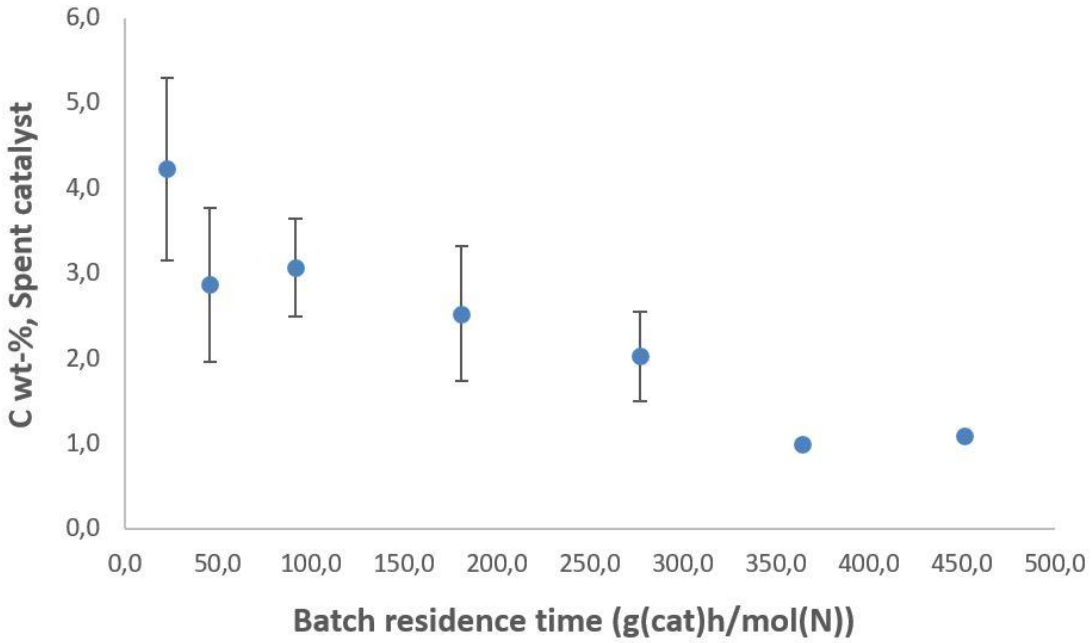

Figure S8: Carbon content analysis results for spent catalysts used for didodecylamine (secondary amine) hydrotreating. Vertical bars show the standard deviation for repeated measurements. Note that the standard deviation is very low (< 0.1 C wt-%) for the samples with a batch residence time over 350 g(cat)h/mol(N).